RI 8263

Bureau of Mines Report of Investigations/1978

The Diffusion Flame in Free Convection

Buoyancy-Induced Flows, Oscillations, Radiative Balance, and Large-Scale Limiting Rates

UNITED STATES DEPARTMENT OF THE INTERIOR

Report of Investigations 8263

The Diffusion Flame in Free Convection

Buoyancy-Induced Flows, Oscillations, Radiative Balance, and Large-Scale Limiting Rates

By M. Hertzberg, K. Cashdollar, C. Litton, and D. Burgess

UNITED STATES DEPARTMENT OF THE INTERIOR
Cecil D. Andrus, Secretary

BUREAU OF MINES

This publication has been cataloged as follows:

The diffusion flame in free convection :
buoyancy-induced flows, oscillations, radiative balance, and large-scale limiting rates / by M. Hertzberg ... [et al.] [Washington] : U.S. Dept. of the Interior, Bureau of Mines, 1978.

33 p. : ill., diagrams ; 27 cm. (Report of investigations - Bureau of Mines ; 8263)

Bibliography: p. 32-33.

1. Flame. 2. Heat - Convection. 3. Mine fires - Prevention and control. 4. Fire-testing. I. Hertzberg, Martin. II. United States. Bureau of Mines. III. United States. Bureau of Mines. Report of investigations - Bureau of Mines ; 8263.

TN23.U7 no. 8263 622.06173

U.S. Dept. of the Int. Library

CONTENTS

ILLUSTRATIONS

TABLE

THE DIFFUSION FLAME IN FREE CONVECTION

Buoyancy-Induced Flows, Oscillations, Radiative Balance, and Large-Scale Limiting Rates

by

M. Hertzberg,[1] K. Cashdollar,[2] C. Litton,[2] and D. Burgess[3]

ABSTRACT

This Bureau of Mines report describes experimental and theoretical studies of diffusion flames in free convection. The cross-coupling between buoyancy-induced flows and the combustion process is explored as it relates to the size, structure, and radiative balance of flames. New data are presented for the size-dependent radiance oscillations of diffusion flames and for the angular distribution of the total radiant intensity from a small methanol pool flame. Both amplitude and frequency of the measured oscillations are compared with theoretical predictions that are based on a new view of the structure of diffusion flames. This new view, which is at variance with the traditional one, assumes uniform reaction in the diffusive mixing zone, and recognizes the significance of the role played by convective buoyancy and its duality in both aiding and impeding flame propagation. Buoyancy quenches propagation at low burning velocities, introducing a real discontinuity in the combustion rate. A "flammable volume" is thus defined as that bound between lean- and rich-limit contours. However, in the flow disturbances generated by combustion waves that consume that volume, buoyancy aids propagation by promoting the convective mixing of a new flammable volume. The measured radiance oscillations are manifestations of these propagation and remixing cycles.

INTRODUCTION

A major problem in developing infrared sensors for the detection of mine fires or explosions is distinguishing a real flame source from other environmental infrared sources that could cause a sensor to false-alarm. These environmental or ambient sources could be incandescent lights, motor castings, or other machinery surfaces that are heated either by friction or by ohmic dissipation. One method of distinguishing between a real flame and such false sources uses the flicker or oscillation characteristics of the flame. The flicker phenomenon raises several interesting questions. What causes the

[1]Research chemist.
[2]Research physicist.
[3]Research supervisor.
All authors are with the Pittsburgh Mining and Safety Research Center, Bureau of Mines, Pittsburgh, Pa.

flicker? How large in amplitude are the oscillations? What is the spectrum of oscillation frequencies? Which flicker frequency or range of frequencies should an infrared flame sensor be tuned to? The Bureau of Mines, as part of its program on evaluating mine fire detection systems, made a brief experimental study of the problem, and attempts to understand the data led to some surprising insights into the fluid dynamics of freely convecting diffusion flames.

ACKNOWLEDGMENT

The authors wish to thank Alex Strasser for his help in making the radiance measurements and in analyzing the data.

THE CLASSICAL LAMINAR-DIFFUSION FLAME

The classical laminar-diffusion flame consists of a stream of fuel flowing from a cylindrical tube into a surrounding air stream of infinite extent. Mixing across the initial fuel-air boundary is generally assumed to occur by pure molecular diffusion. The presence of the flame is assumed to exert no influence on the fuel-air mixing process that occurs upstream. The shape of the flame is assumed to be controlled only by the geometry of the fuel supply tube, the initial flow velocity field, and the interdiffusion coefficient. For steady-state conditions, the conservation equation for fuel molecules in the upstream mixing region is

$$\vec{\nabla} \cdot \left(X_f \, \vec{v} \right) = D\nabla^2 \, X_f \,, \tag{1}$$

where X_f is the fuel mole fraction, $\vec{v}$ is the velocity, and D is the coefficient of diffusion.

The simplest configuration to consider is that of a cylindrical stream of fuel of initial radius r flowing parallel to a surrounding air stream of infinite extent. If the axial flow velocity of both gases is everywhere equal to $|\vec{v}| = v_z$, the steady-state diffusion equation in cylindrical coordinates reduces to

$$\frac{\partial x_1}{\partial z} = \frac{D}{v_z} \left[\frac{\partial^2 x_1}{\partial r^2} + \frac{1}{r} \frac{\partial x_1}{\partial r} \right]. \tag{2}$$

This problem was studied by Burke and Schumann (6),[4] who obtained exact solutions to equation 2 for a fuel stream of radius r_o flowing concentrically within a confined air stream of larger radius. An approximate, averaged solution in simplified form for the unconfined case may be presented as follows.

Initially, at z = 0, pure fuel ($X_f = 1$) issues from the fuel tube between r = 0 and $r = r_o$. It flows parallel to a surrounding air stream. For an

[4]Underlined numbers in parentheses refer to items in the list of references at the end of this report.

air stream of infinite extent (an overventilated flame), the fuel stream is continuously diluted by diffusion as it travels parallel to the air stream. Eventually at some infinite distance, $z = \infty$, it is diluted to $X_f = 0$. Typical solutions to such diffusion equations for the decay of concentration across some characteristic dimension δ during some traveltime t are of the form

$$\frac{X_f(t)}{(X_f)_o} = e^{-t/\tau_{diffusion}}, \tag{3}$$

where $\tau_{diffusion} = \frac{\delta^2}{4D}$.

For a cylindrical stream of initial radius r_o, the characteristic dimension δ is taken as the area-weighted average distance to the initial stream boundary, which gives $\delta = \frac{2}{3} r_o$. Since $t = z/v_z$, and since $(X_f)_o = 1$ at $t = 0$, we have

$$\bar{X}_f = \exp\left(-\frac{9Dz}{v_z r_o^2}\right), \tag{4}$$

where $\bar{X}_f$ is the average fuel concentration at any axial distance z within the initial circular fuel stream boundary. One typically characterizes the diffusion flame in terms of some flame height, which is associated with some characteristic average fuel concentration $(\bar{X}_f)_h$. This gives

$$z_h = \frac{v_z r_o^2}{9D} \ell n \frac{1}{(\bar{X}_f)_h}. \tag{5}$$

Burke and Schumann defined their flame heights to be the distance between the fuel port and the top of the luminous zone. They associated this luminous zone with the position of the flame front at $r = 0$, which was taken to coincide with the stoichiometric value of X (which for methane is $X_f = 0.095$). They performed a variety of empirical tests to verify their simple theory. The flame height for a given fuel was observed to be independent of tube dimensions if the total flows of gas and air were kept constant. This is as predicted by equation 5 since the fuel volumetric flow is simply $\pi r_o^2 v_z$. They compared flame heights of CO flames to those of H_2 flames. Based on the ratio of D's, the former should have been a factor of 4 taller than the latter. The measured ratio was 2.5; however, it is difficult to know precisely what relative values of $(X_f)_h$ to choose in making such a comparison. For stoichiometric values, the $\ell n \frac{1}{(\bar{X}_f)_h}$ factor would be the same for both flames. However, for lean-limit values of $\bar{X}_f$, the predicted height ratio would be very close to their measured value of 2.5. They also verified that flame heights were proportional to v_z, as indicated by equation 5. They studied the effects of changes in initial fuel concentration and equivalence ratio, and the measured dependences were qualitatively similar to those predicted by the laminar solutions. They varied pressure and found no effect, as predicted, since both D and v_z vary inversely with pressure.

Yet despite the apparent agreements, Burke and Schumann clearly indicated that the use of independently measured D values does not properly predict the absolute magnitude of flame heights or the concentration profiles. They measured the z-dependence of concentration along the axis of CO diffusion flame. Agreement between measured and calculated axial profiles was obtained only if D_{CO-air} was taken to be 0.67 $cm^2 sec^{-1}$ rather than its standard value of 0.19 $cm^2 sec^{-1}$.

Subsequent research by Hottel and Hawthorne (13) and Wohl, Gazley, and Kapp (20) involved studies of fuel streams flowing into initially quiescent air at velocities that extended well into the turbulent flow regime. For such flames, mixing was controlled by turbulent eddy diffusion. Barr (2) studied the structure and stability of diffusion flames in an enclosed cylindrical burner similar to that used by Burke and Schumann; however, fuel and air flows were varied over four orders of magnitude. In addition to the normal structures of overventilated and underventilated flames, a variety of additional structures were observed, both steady and oscillatory; and a variety of extinction limits were attained.

Barr clearly recognized that the application of equation 2 to the enclosed cylindrical burner system was an oversimplification because it neglected the problem of momentum transfer between the fluid streams. The Burke and Schumann solutions assumed that the quantity v_z in equation 2 was constant and independent of r and z, whereas the real velocity profile in the concentric tube system is dependent on both coordinates. This is clearly illustrated in figure 1, where the typical enclosed cylindrical burner is depicted together with its overventilated flame as observed by Burke and Schumann (their figure 6, with flame and geometry from their table I). The laminar flow profile at the burner exit, z = 0, is shown together with the velocity profile at some distance well above the fuel inlet. These profiles were calculated for the geometry and volumetric flow given in their table I (neglecting the finite wall thickness of the fuel tube). Clearly, the initial velocity in the boundary region between the fuel and air streams (at r = 0.476 cm) is initially zero at z = 0, and must increase continuously to attain its final value in the fully developed Poiseuille flow profile. This requires substantial momentum exchange from the outer to the inner stream in all regions of the initial fuel-air boundary. There is also substantial initial vorticity in the velocity gradients at z = 0 and r = 0.467. Clearly, v_z must be strongly dependent on both r and z throughout the mixing zone. In addition the velocity field must contain substantial radial components. It would appear to be unreasonable therefore to exclude the possibility of radial convective mixing in a region of significant initial vorticity undergoing substantial radial momentum exchange. In any case, even in the absence of such convective mixing, the X_f contours must compress inward with the inward momentum transport.

These fluid dynamical aspects of the problem were studied by Savage (17), who compared the measured flame shape with those predicted by the constant-flow solutions of Burke and Schumann. He observed that despite the fact that the calculated concentration profiles (for a stoichiometric mixture) should extend radially well beyond the projection of the burner tube at r_o, the

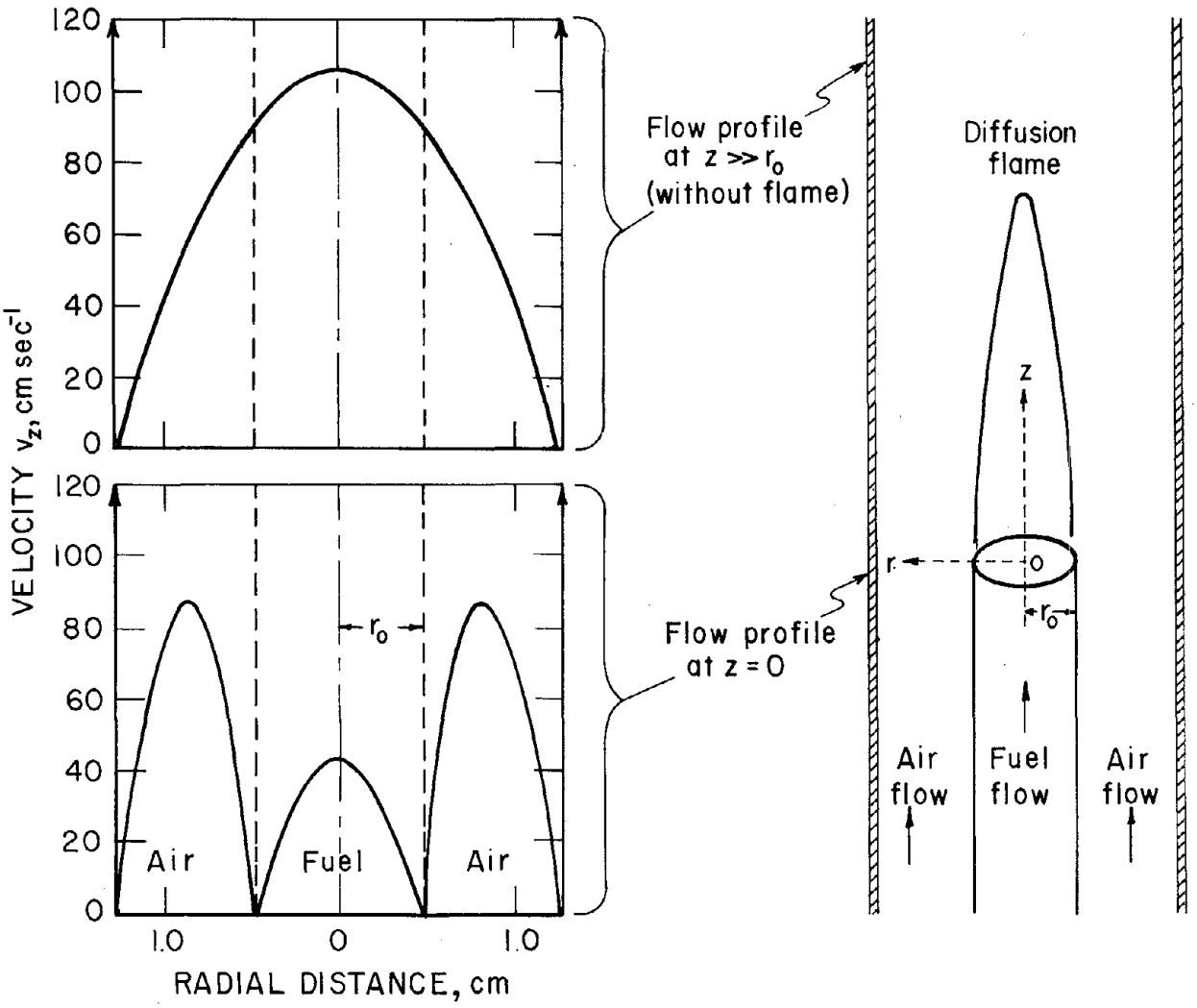

FIGURE 1. - The classical laminar-diffusion flame. Initial and final velocity profiles, illustrating the inward momentum transport required in the diffusive-mixing zone.

observed flame shapes are invariably confined to within r_o. This observation shows that the inward radial transport of momentum required by the velocity profiles of figure 1 is significant to the point of dominance. He concluded that, in addition to the quantitative disagreement in the magnitudes of the D's required, the classical solution of Burke and Schumann, which neglects radial momentum transport, does not fit the experimentally measured flame profile contours in the regions where stable flames are obtained.

It should be noted, however, before leaving this aspect of the problem, that it is possible to generate constant-velocity flow profiles with either a Mache-Hebra nozzle or a porous plug burner similar to those used extensively in structure studies of premixed flames. Radial momentum exchange and axial velocity dependences can be made negligible in the central regions of

such burners; hence, the exact solutions to equation 2 should indeed be accurate descriptions of concentration profiles provided those types of burners are used.

Now in addition to the aforementioned problems, the presence of a combustion zone can have a significant effect on the cold gas flow structure upstream of the flame zone. Although it is generally assumed that the flame reaction occurs instantaneously at the stoichiometric concentration contour surface, there is probably no reason to expect that reaction should not actually start at the X_ℓ contour surfaces that correspond to the rich and lean limits of flammability at the temperatures involved. From this viewpoint, the rich- and lean-limit contour surfaces are the boundaries of a flammable volume of finite size. While the traditional view is that reaction proceeds uniformly and in steady state throughout that volume, there is an alternative viewpoint, which is that the process can be oscillatory in nature, with a contiguous wave traveling through that flammable volume and consuming it at a rate that need not precisely match its rate of generation by the flow field. If one admits of the possibility of continguous combustion waves traveling through portions of the flammable volume in ignition, propagation, and reignition cycles, while the complementary portions of that volume are being regenerated by diffusive or convective mixing, then clearly oscillatory solutions to the problem are likely. In addition, it also becomes likely that the combustion and mixing processes will be cross-coupled.

The presence of the combustion process then introduces two new and clearly distinguishable internal forces into the problem. These forces should be added to the inertial and viscous forces that are present in the unburned or unignited cold gas flow structure. One force is the combustion force, which is the gradient of the kinetic energy increase per unit volume across a propagating flame zone; the other force is the buoyancy force couple. Both are internal sources of flow and can exert profound effects on the flow field and the mixing process.

THE BUOYANCY FORCE COUPLE

The Maximum Buoyant Rise Velocity

It is possible to obtain some reasonable insight into the nature of the buoyancy force and the effect it may have on the flow structure by considering the simplest example: an idealized, spherical combustion wave propagating into a premixed gas of uniform composition in a gravitation field.

The buoyancy force per unit volume is ρg. Because there is a density gradient between the burned gas within the fireball (ρ_b) and the unburned gas in the surroundings (ρ_u), buoyancy induces a force gradient, and flame propagation in buoyancy-induced flows inevitably produces distortions in flame shape. In the simplest example, the detailed distortions are ignored, and the inquiry centers on determining the rise velocity of the fireball's center of mass as the system responds to the buoyancy force.

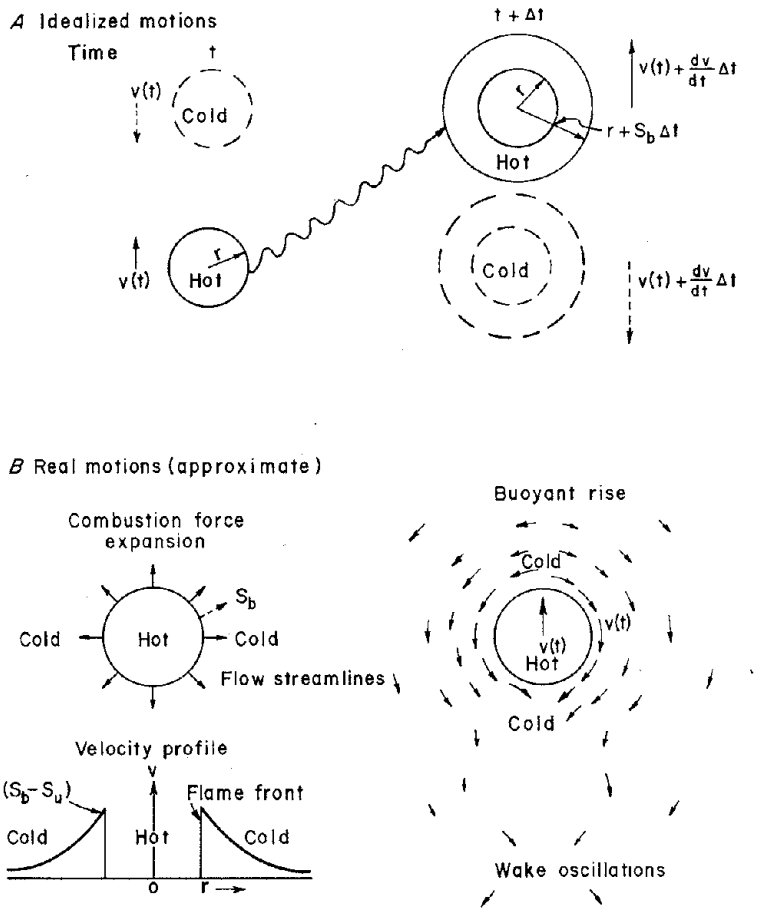

FIGURE 2. - Idealized motions for the maximum buoyant rise velocity of a spherical combustion wave and real motions shown as the composite of the combustion force expansion and the buoyancy force couple.

The situation is depicted in figure 2. At some initial time t, a fireball of radius r(t) is rising upward by buoyancy at a velocity v(t). At some time $t + \Delta t$ later, the fireball has expanded to a new radius $r + S_b \Delta t$, and its new buoyant rise velocity is $v(t) + \frac{dv}{dt} \Delta t$. The quantity S_b is the spherical flame speed relative to the laboratory observer. The buoyancy force acts simultaneously on both the burned product fireball and the unburned reactants that surround it. The momentum change induced by buoyancy must involve not only the upward motion of burned products, but also the simultaneously induced downward motion of the unburned gases, since the cold surroundings must descend to fill the space vacated by the fireball. An equivalent volume of the cold surroundings is also idealized and shown in figure 2A. It is depicted as separated from the fireball, expanding in size as the fireball does, and descending at an identical velocity. The western hemisphere of the fireball moves upward as its surroundings descend, introducing a moment of force or torque about the equatorial axis, which generates a continuous cyclonic vorticity about the rising fireball. With the eastern hemisphere, the continuous vorticity is anticyclonic. Since these motions of fireball and surroundings are coupled and involve a moment of force or torque, they are referred to as being induced by the buoyancy force couple.

In reality, the motion of the surroundings is necessarily more complex, as depicted in figure 2B where the motions are viewed in a coordinate system moving upward with the fireball. There is first a continuous outward motion induced by the combustion force expansion. At the flame boundary, the unburned gas recedes at a velocity $S_b (1 - \rho_b/\rho_u)$, and this radial velocity decreases with the inverse square of the dimensionless distance from the

center of the fireball. Superimposed on this expansion are the buoyancy-induced flows. Near the top of the fireball the surroundings must move outward, parting from the upward path of the fireball. In the equatorial regions, the motion is downward as required by the buoyancy force. Near the bottom of the fireball, the motion is inward, to fill the space being vacated by the bottom of the rising fireball. In the idealization of figure 2A, it is assumed that the buoyancy components of the outward motions at the top, and inward motions at the bottom, are canceled exactly, so that no other motions are induced but those necessary to raise the expanding fireball upward at v(t) and to simultaneously displace an equal volume of the surroundings downward at the same velocity. Any additional buoyancy-induced motions that appear either with the fireball or in the surroundings (as in a wake) should be treated as a drag force that would retard the rate of rise. Accordingly, this derivation is that of the maximum buoyant rise velocity in initially stationary surroundings.

With respect to the laboratory coordinate system (fig. 2A), the change in the momentum of the system between time t and time t + Δt is given by

$$\Delta mv = \overbrace{\left[v(t) + \frac{dv}{dt}\,\Delta t\right]}^{a} \overbrace{\frac{4}{3}\,\pi\left\{(r+S_b\Delta t)^3\,\rho_b + r^3\rho_u + \left[(r+S_b\Delta t)^3 - r^3\right](1-\rho_b/\rho_u)\rho_u\right\}}^{b}$$

$$\underbrace{-v(t)}_{c}\ \underbrace{\frac{4}{3}\,\pi\left\{r^3\rho_b + r^3\rho_u\right\}}_{d}. \qquad (6)$$

The term a is the final velocity and b is the final mass of gas moving, so that the product is the final momentum. The term c is the initial velocity and d is the initial mass of gas moving, so that their product is the initial momentum. Both initial and final masses of moving gas comprise the sums of the hot gas ascending and the cold gas descending. In b, the final mass of cold gas that is descending is shown in two parts: the initial mass plus the new mass required, corrected for that fraction that is lost to the fireball.

For spherical propagation, the vector sum of the radial combustion forces acting on the fireball is zero. Accordingly, in the limit as t→0, this rate of change of momentum is equated to the buoyancy force.

$$\lim_{\Delta t\to 0} \frac{\Delta(mv)}{\Delta t} = \frac{d(mv)}{dt} = (m_{cold} - m_{hot})\,g. \qquad (7)$$

Neglecting terms of higher order in Δt, one obtains the differential equation

$$\frac{dv}{dt} + \frac{3v}{t}\left(\frac{\rho_u}{\rho_u + \rho_b}\right) = \left(\frac{\rho_u - \rho_b}{\rho_u + \rho_b}\right) g. \qquad (8)$$

Multiplying the equation by $t^3\eta$, where $\eta = \frac{\rho_u}{\rho_u+\rho_b}$, the left-hand side of the equation becomes an exact differential, and the solution is

$$v_b(t) = \frac{1}{1+3\left(\frac{\rho_u}{\rho_u+\rho_b}\right)} \left(\frac{\rho_u - \rho_b}{\rho_u + \rho_b}\right) gt. \tag{9}$$

It is interesting to compare the predictions of this equation with the data reported by Sapko, Furno, and Kuchta (16). They have measured the buoyant rise velocities for fireballs as function of size (and time) for homogeneous mixtures of methane in air. For an intermediate range of methane concentrations (6.5% to 8.5%) their measured values average out to give

$$v_b \text{ (measured) (cm sec}^{-1}) = 182\ t^{0.70} \text{ (sec)}. \tag{10}$$

Substituting an average value for the expansion ratio $\rho_u/\rho_b = 6.3$ into equation 9 and setting $g = 980$ cm sec^{-2}, one obtains

$$v_b \text{ (calculated)} = 198\ t. \tag{11}$$

The agreement is thus fair in these regions of intermediate concentration. Mixtures of near-stoichiometric compositions generate large fireballs so rapidly that it is difficult to accurately locate and track their center of mass, whereas for the near-limit mixtures, there are severe distortions in fireball shape and significant ignition-induction delay times. Apart from such measuring inaccuracies, the remaining discrepancy between the calculated and measured buoyant rise velocity is attributable to the neglect of additional buoyancy-induced motions within the fireball or in its wake. These drag forces retard the observed rate of rise, and the measured values are logically somewhat smaller than the calculated values. As indicated earlier, the calculated value should represent the maximum possible rate of rise. The theoretical value of 198 cm sec^{-2} for the upward acceleration gives excellent agreement with the measured slopes of Margolin, Karpov, and Severin (15). Their data were obtained in small vessels for lean mixtures at several pressures. Good agreement is also obtained between equation 11 and their measured absolute displacements, provided one is careful to correct for the initial upward displacement of the spark bubble during an ignition delay period of 0.07 sec.

Now the flow structure and geometry of a diffusion flame are significantly different from those of a spherical combustion wave propagating into a premixed gas. However, as indicated earlier, one may view diffusion flames as contiguous combustion waves rather than as systems in which reactions proceed uniformly throughout the volume. This alternative to the traditional view is that combustion waves travel through a flammable volume which is formed by mixing in the upstream flow regions. Contiguous waves propagate through the volume in mixing, ignition, propagation, remixing, and reignition cycles. This view is capable of explaining many of the observed effects, particularly those that are displayed by the larger scale diffusion flames.

Accordingly, one associates the spherical fireball of figure 2 with the burned gas volume being generated by the flammable volume contained between the lean- and rich-limit contours of the diffusive mixing zone. (Such a flammable volume is depicted in figure 8.) The formula derived may then provide some insight into the magnitude of the convective rise velocity generated at the base of the diffusion flame plume. Similarly, the fireball radius r would be associated with the dimensions of the flame and would be either the radius of a liquid pool flame or the radius of a fuel gas stream.

The Buoyancy-Induced Reynolds Number

It is possible to obtain some general estimates of flow behavior in terms of a buoyancy-induced Reynolds number: $R = \frac{2v_b r}{\nu}$, where r is now the radius of the fireball and ν is the kinematic viscosity. Substituting the approximate expression from equation 9

$$v_b \simeq \frac{1}{4} \left(\frac{\rho_u - \rho_b}{\rho_u + \rho_b} \right) gt \tag{12}$$

into the Reynolds number definition and setting

$$t = \frac{r}{S_b} = \frac{r}{S_u} (\rho_b / \rho_u)$$

gives

$$R = \frac{1}{2} \frac{gr^2}{\nu S_u} \left[\frac{1 - \rho_b / \rho_u}{1 + \rho_u / \rho_b} \right]. \tag{13}$$

For the development of turbulence in the fireball boundary layer, one sets $R_{crit} = 3 \times 10^5$ (18). Now for a diffusion flame, r is associated with the pool radius r_o. The flammable volume concentration is assumed to average out to a near-limit mixture: a rich limit mixture near the fuel space and a lean-limit mixture near the air space. The limit expansion ratio is $\rho_u / \rho_b = 5$ and S_u is taken as the limit burning velocity for horizontal propagation (9), $S_u = (S_u)_a = 6.0$ cm sec^{-1}. This gives

$$r_{crit} \simeq 70 \text{ cm}. \tag{14}$$

Thus pools of radii larger than this value would be characterized by turbulence in the mixing zone above the surface of the liquid pool. These are about the dimensions at which pool flames do indeed become turbulent (12).

It is important to realize that one is not here dealing with the type of turbulence that develops high up in the buoyant plume, far removed from the source of buoyancy. Rather, this type of turbulence is in the boundary layer of the fireball, which in the case of the pool flame corresponds to the very source of buoyancy in the flammable volume nearly adjacent to the pool surface. This turbulence induces rapid convective mixing of fuel and air streams. This convection is far more effective in generating the flammable volume than pure molecular diffusion. It is also important to recognize that the fluid dynamics of this process are not adequately characterized by the

Grashof number. An essential parameter, the burning velocity S_u, which represents the strength of the combustion force, is missing from the Grashof number description of the phenomenon.

DIFFUSION FLAME FLICKER AND RADIANCE OSCILLATIONS

Previous Studies

Early studies of the flicker of luminous, free diffusion flames were reported by Chamberlin and Rose (8), who used photographic methods to measure and track various time-dependent structural features. Their data showed that the upper portion of the luminous zone oscillated between a maximum and a minimum height about 10 times per second. This vibration frequency appeared to be insensitive to type of fuel but did depend somewhat on volumetric flow and fuel orifice dimensions. Barr (2) varied fuel and air flows independently in an enclosed cylindrical diffusion flame burner similar to that used by Burke and Schumann (6). He observed a variety of oscillatory structures and limit conditions when flow velocities were varied over four orders of magnitude. One type of oscillatory structure described by Barr, for an overventilated laminar flame of butane in air, was similar to that described by Chamberlin and Rose. Barr's frequencies were in the 8-Hz range, and the oscillatory structure started with an inward "necking" or pinching of the flame. This progressed until the upper portion separated from the lower portion, rising upward and burning independently from the lower "anchored" portion of the flame. The oscillation frequency could be varied between 3 and 20 Hz by varying the fuel supply system. Barr suggested that the oscillations were associated with variations in the fuel supply rate but that these variations were self-excited rather than forced. Maklakov (14) has also studied such oscillatory structures. He indicates that the oscillations are simply periodic if the gas flow exceeds some critical value which depends on burner size, flow inclination to the vertical, and type of fuel. Similar oscillations were observed over liquid pool flames. Since the oscillations were independent of length of inner fuel supply tube or outer tube dimensions, he agrees with Barr that the oscillations are free and self-exciting rather than forced. Maklakov suggests that they are caused by internal changes in the conditions of mixing. Combustion products generated in the lower portion of the flame, near the mixing edge, shield the central regions of the fuel stream from the air stream, causing the combustion rate to slow down and the flame length to increase. The resultant decrease in combustion rate lowers the concentration of combustion products, which increases the rate of mixing, which shortens the flame length. This increase in burning rate generates more combustion products, which again shield the central regions of the fuel stream, lengthening the flame and restarting the cycle. Blinov and Khudiakov (3) report flame oscillations in the 10- to 15-Hz range for gasoline pool flames with diameters larger than a critical value in the centimeter range, below which the flames appear steady. The structural features associated with the oscillation were observed to change with increasing diameter. The oscillation frequency tends to decrease with increasing pool diameter, and the upper flame tends to break away from the lower regions at these larger diameters. For very large diameters the oscillations appear randomly distributed in time and space, and the flame appears turbulent. Even for the smaller, periodically oscillating

structures, the flow in the upper regions of the flame plume can appear turbulent. This is explained by them in terms of the flow structure of a buoyant plume whose Reynolds number increases with height above the source. Hertzberg (10) has suggested that these diffusion flame oscillations are manifestations of ignition, propagation, mixing, and reignition cycles within some finite flammable volume above the liquid fuel surface. The flammable volume is that volume bounded by the lean- and rich-limit contour surfaces. Ignition of this volume causes a combustion wave to travel through it at a finite rate and to generate combustion products, whose expansion temporarily inhibits the entrainment of air and its diffusive or convective mixing with fuel. It is not until these products are convected upward by inertial and buoyancy forces that fresh fuel and air volumes can mix to generate a new flammable volume. A time delay is thus required for the regeneration of this new flammable volume. Once formed, the new volume is reignited, generating a new combustion wave, which restarts the cycle. The fuel-air entrainment and mixing process is probably cross-coupled to the buoyancy-induced flow structure. This cross coupling should cause the oscillation frequency to increase at high g-values and to decrease at low g-values. Altenkirch, Eichhorn, and Hsu (1) are currently studying the influence of elevated gravity on the overall structure of laminar diffusion flames. They recently reported such increases in oscillation frequency with increasing g.

Byram and Nelson (7) measured the oscillation frequency of pool flames of 95% ethanol. These pools ranged in size from 0.5 ft (15 cm) to 8.0 ft (244 cm) in diameter. They indicated that the rhythmic pulsation of flames appeared most readily for circular pools and were most pronounced in quiet, stable air. Their measured frequencies decreased with increasing diameter: from 3.5 Hz for the 15-cm pool to 1.0 Hz for the 244-cm pool. For the smaller diameter pool flames the frequencies were measured photographically. For the larger pools frequencies were measured acoustically by counting the number of maxima in the roaring sounds per unit time.

The Infrared Radiance Oscillations of Methanol Pool Flames

The oscillations in visible flame height and structure are also associated with changes in the volume and/or temperature of combustion products generated by the flame zone. Thus, these flame structure oscillations are also reflected in the infrared radiance associated with these burned-gas products. The data in figure 3 show the time-dependence of the spectral radiance of the 2.8-μm H_2O band emitted from the burned gas products of methanol pool flames. The relative radiance is shown as a function of time for pools of diameter varying from 3.9 cm to 33.3 cm. The relative radiance was measured with an InAs photodetector and an interference filter centered on the 2.8-μm emission band of H_2O. The detector viewed the flame horizontally at a distance of many pool diameters from the source. The data for the smallest pool show a low-amplitude radiance oscillation at a frequency of 12.8 Hz, whereas the largest diameter pool flame shows a rather large amplitude oscillation at 2.20 Hz.

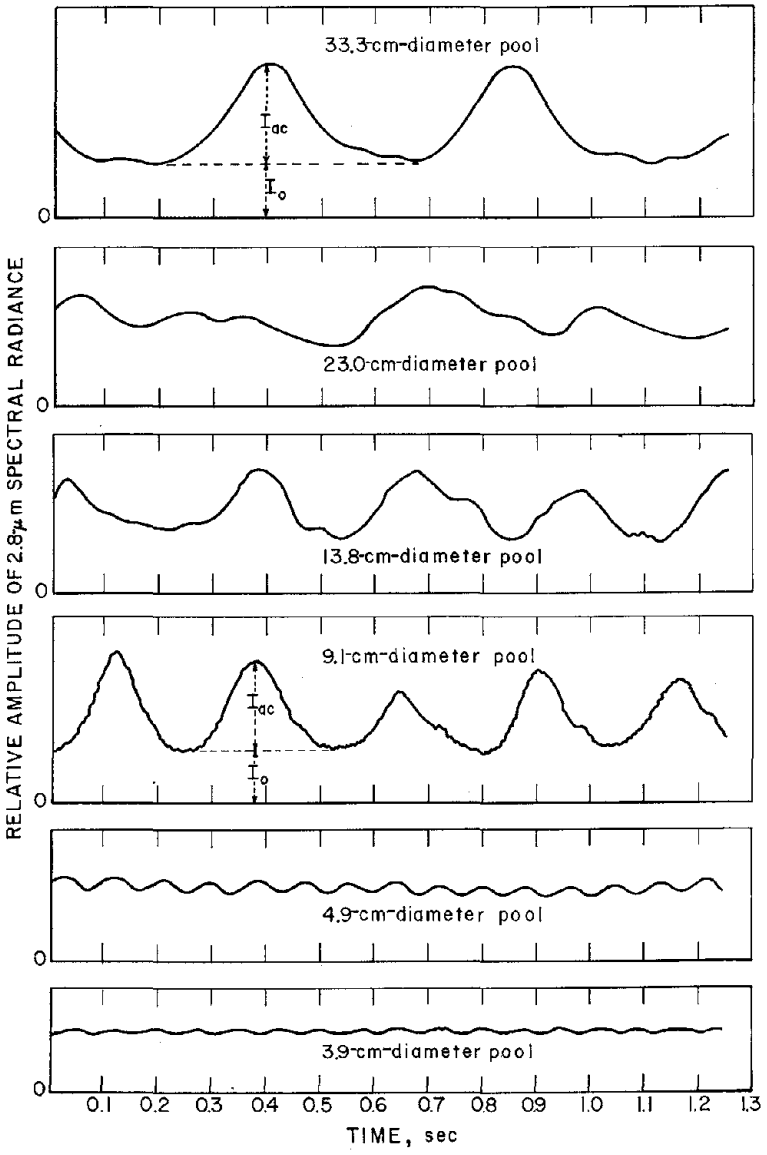

FIGURE 3. - Time dependence of the spectral radiance of the 2.8-μm H_2O band emission from methanol pool flames of varying diameters.

The fundamental oscillation frequency and the average oscillation amplitude ratio I_{ac}/I_o are plotted as a function of pool diameter in figure 4. There is a monotonic decrease in frequency with increasing pool diameter, whereas the oscillation amplitude shows a rapid increase at diameters above 5 cm and levels off at a nearly constant value for the larger diameters. An inspection of the radiance curve for the 23-cm-diameter pool reveals that it contains more frequencies than the others. This is reflected in its lower amplitude ratio, I_{ac}/I_o, which is plotted in figure 4. It is possible that fluid flow conditions were less stable for that particular system, causing edge flow or vortex instabilities that were anomalously large. The fuel container, in that instance, was a pie pan whose diameter increased from 20.5 cm near the bottom to 25.6 cm at the upper lip. It is possible that this flaring out of the side wall of the pool encouraged the development of edge flow instabilities. For the other diameters, the container walls were vertical. This lower amplitude of oscillation for the 23-cm-diameter pool was accordingly ignored in the smooth curve in figure 4. The data for the 9.1-cm pool displayed the most rhythmic oscillations and the largest amplitude of the fundamental. Figure 5 is a Fourier transform of its radiance signal for an 8-sec interval and clearly shows the narrow-band peak at 3.85 Hz. Some low-amplitude higher frequencies also appear, as does a lower frequency modulation at half the fundamental. A similar Fourier transform of the 33.3-cm-diameter pool flame signal clearly revealed the fundamental at 2.20 Hz; however, the higher and lower frequency modulations were also present.

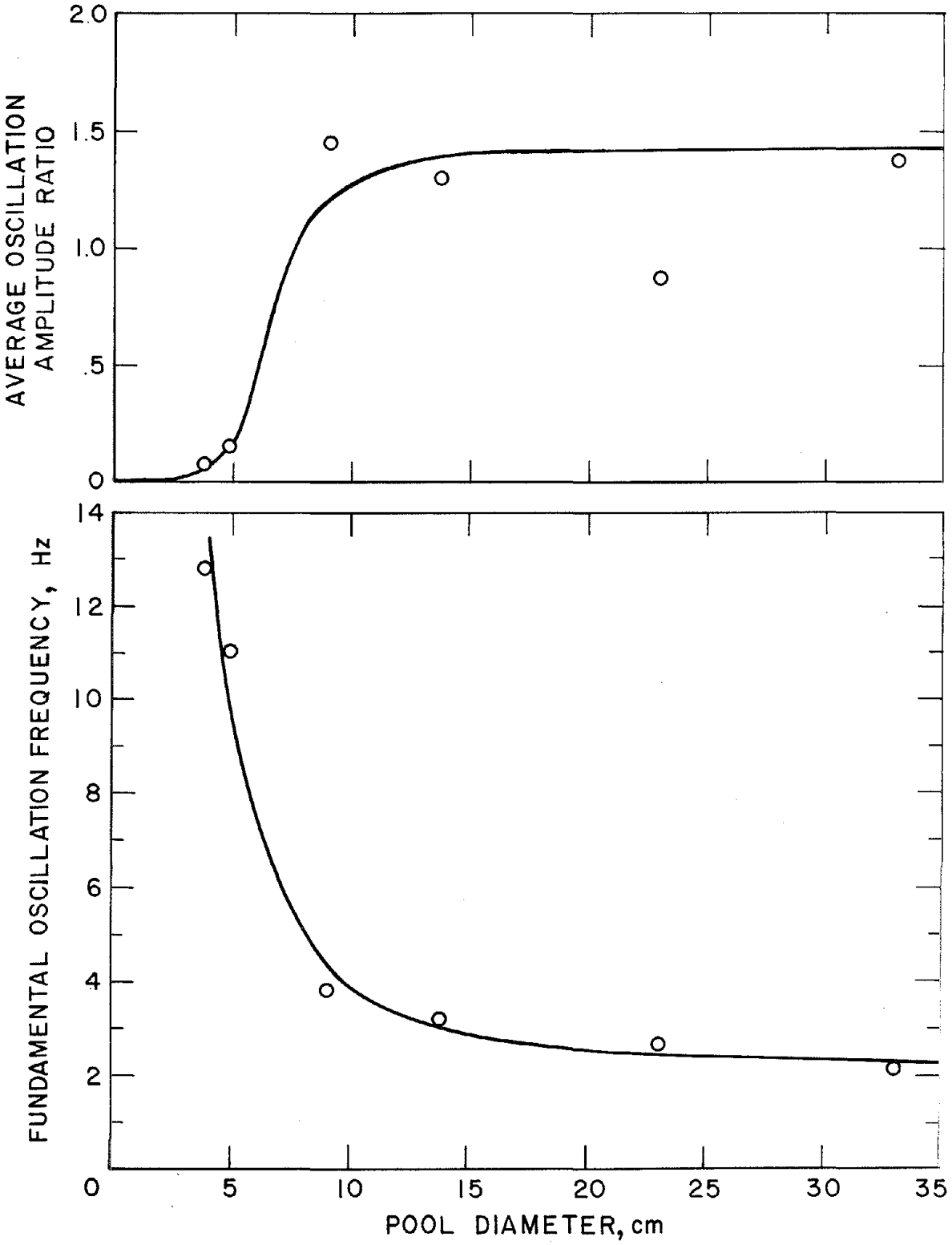

FIGURE 4. - Fundamental oscillation frequency and average oscillation amplitude of the 2.8-μm emission as a function of pool diameter.

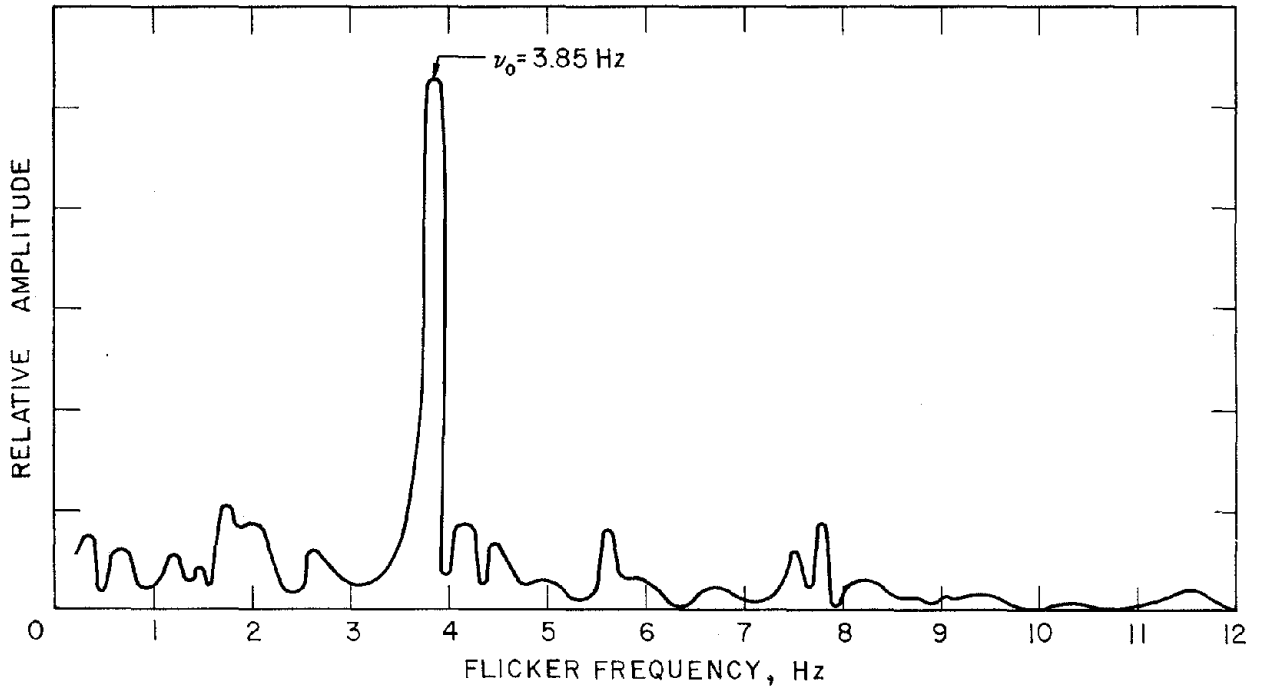

FIGURE 5. - Fourier transform of the radiance signal from the 9.1-cm-diameter methanol pool flame.

These data for methanol flames may be compared with the data of Byram and Nelson (7) for ethanol (95%) pool flames. The comparison in figure 6 clearly shows good agreement in the region of overlap. The methanol frequencies average some 20% higher, possibly reflecting the normal variations associated with differences in the heat-up periods for both measurements. Although it is possible that the differences are caused by the difference in the fuels used, Byram and Nelson noted that changes of this magnitude can occur during the burn-in time.

Recent data by Sibulkin and Hansen (19) for the oscillation frequencies of a spreading flame over a thick fuel bed of polymethylmethacrylate also give good agreement with these data when they are averaged over their size range of 3 to 10 cm.

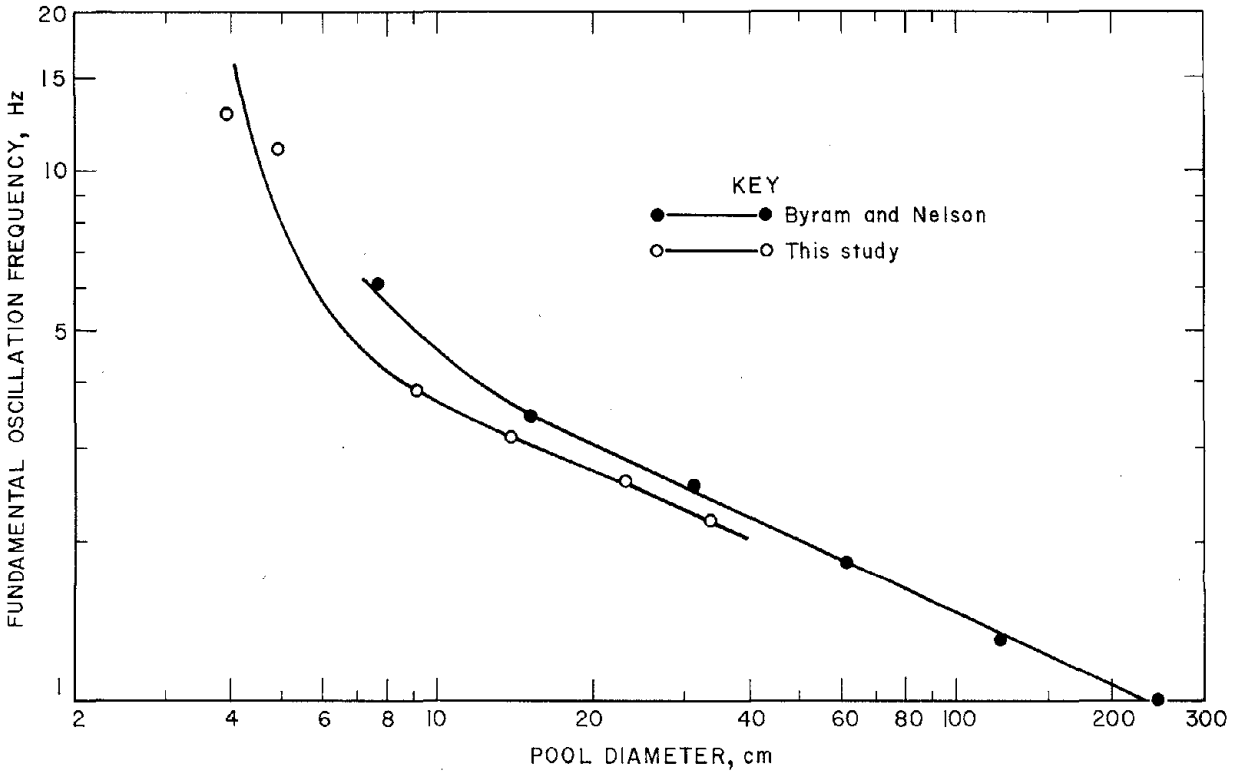

FIGURE 6. - Comparison of the observed frequencies for this study of methanol flames with the data of Byram and Nelson for ethanol pool flames.

Other Flame Oscillations and Phase Lag

In addition to the data for methanol pool flames, infrared radiance oscillation data were obtained for several other diffusion flames. These data are shown in figure 7. The data were obtained simultaneously at two different wavelengths, 1.57 μm and 4.4 μm, using PbSe detectors and interference filters. The shorter wavelength was chosen to be representative of the continuum emission from soot. This continuum is responsible for the visible luminosity, and it is this visible luminosity that is traditionally used to define the flame height. The longer wavelength radiation was at the 4.4-μm CO_2 band emission. This CO_2 band is representative of the highest temperature emission in the burned-gas regions of the flame and usually contains most of the radiant energy for the smaller or "cleaner" flames. As can be seen by comparing figure 4 with figure 7, the fundamental oscillation frequencies are similar to those observed for methanol pool flames of comparable size. The isopropanol flame oscillates in the 3- to 4-Hz range, as did the methanol pool flame of the same size. The 2.5-cm-diameter wood cylinder flame oscillates at a frequency of about 11.5 Hz. Although this is significantly lower than would be expected for a methanol pool of 2.5-cm diameter, the burning area of the wood included part of the sides of the cylinder, in addition to its edge. Based on the total area of wood fuel, this frequency is comparable to what would be expected from a methanol pool of similar area. The natural gas flame

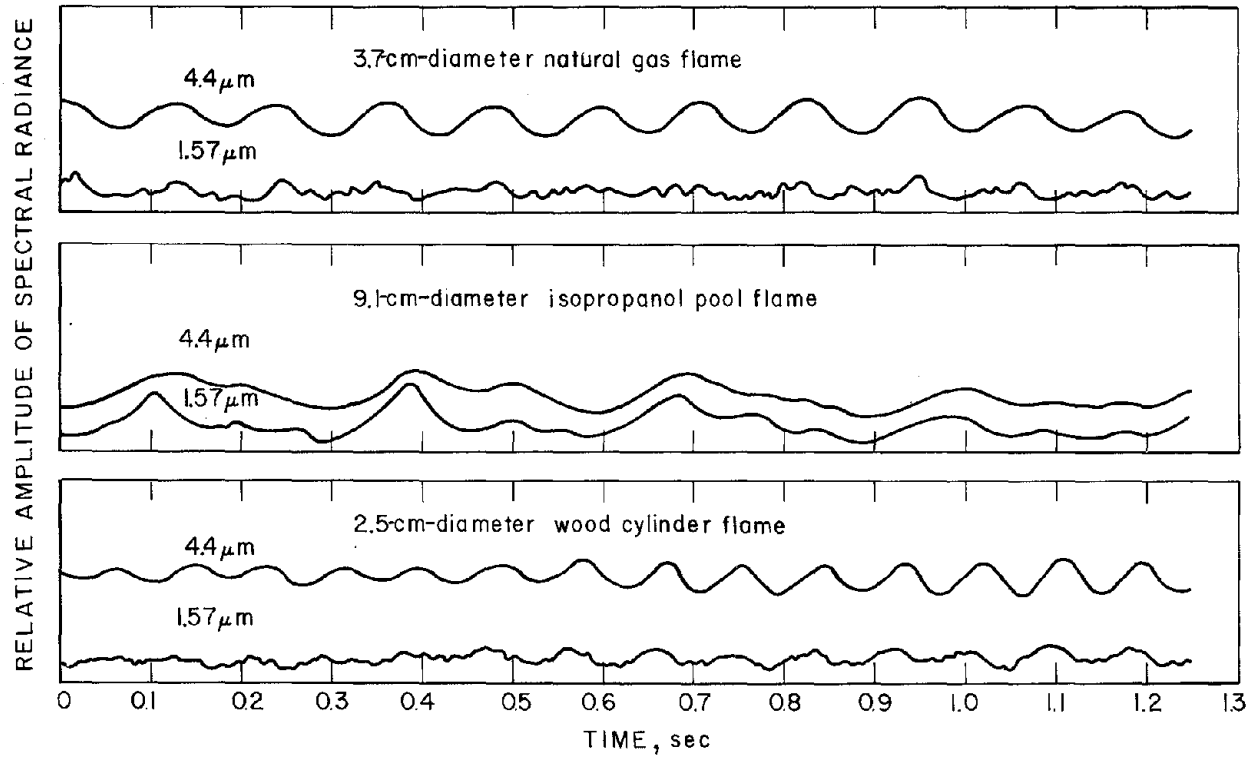

FIGURE 7. - Phase relationship of the radiance signals obtained simultaneously at 1.57 μm and 4.4 μm from several diffusion flames.

from a Meker burner of 3.7-cm diameter oscillates in the 8- to 10-Hz range depending on gas flow rate. This is somewhat lower than the frequency of a methanol pool of comparable diameter, but the burner fuel flow is probably larger than that from the methanol surface.

However, the main purpose of this series of experiments was to determine whether there was any significant phase difference in the oscillation signals at the two wavelengths. A significant phase lag was observed for the wood cylinder flame, where the continuum signal at 1.57 μm preceded the CO_2 band by about 60°±23°. For the isopropanol flame, the phase lag was barely significant with the continuum signal preceding the CO_2 band signal by 27°±16°. For the Meker burner diffusion flame, the continuum signal appears to lag the CO_2 band signal by about 28°±16°. A closer inspection of the isopropanol data also reveals that the continuum signal contains more higher frequencies than the CO_2 signal. This is probably a reflection of the fact that these shorter wavelength emission amplitudes are far more sensitive to temperature fluctuations than the longer wavelength emissions.

Theory, Analysis, and Discussion

A further inquiry, in a more quantitative form, into the causes of these diffusion flame oscillations will now be attempted. This inquiry will attempt to provide some understanding of the factors that control the frequency and

amplitude of the oscillations. The governing rate processes involved are mixing and propagation, and these may be compared in terms of their characteristic times τ_m and τ_p. If $(r_o - r)$ is the radial distance of a fuel stream element from the holding edge of the diffusion flame, then the characteristic propagation time is $\tau_p = (r_o - r)/S_f$, where S_f is the flame speed. (The holding edge is the radial distance, r_o, at which fuel and air streams first meet in the flow.) For the moment we assume that the only mixing process is pure molecular diffusion, and hence for the cylindrical stream the characteristic mixing time to attain some characteristic concentration x is

$\tau_m = \frac{(r_o - r)^2}{kD} \ln \frac{1}{x}$, where k is a geometric constant.

The ratio of mixing to propagation times is therefore

$$\tau_{mixing}/\tau_{propagation} = \frac{(r_o - r)S_f}{kD} \ln \frac{1}{x} \qquad (15)$$

and is proportional to the distance of the fuel stream from the holding edge. For small-diameter flames this τ-ratio is always small, and mixing times are fast enough so that the flammable volume is everywhere generated more rapidly by diffusion than it can be consumed by the propagation wave. The flammable volume is thus effectively premixed at all times, and a combustion wave can be continuously maintained in steady state at the upper boundary of that volume. The steady-state wave is continuously balanced against the flow structure of the incoming flammable volume (as it is in a premixed bunsen burner flame). However, since different degrees of mixing have occurred at different r-values, and since S_f is a function of the mixing ratio, the burning velocity is itself a function of r and the steady-state flame angle is determined by both the flow profile and the composition profile. This structure is the stable or steady diffusion flame which displays little or no flame oscillations. This structure also describes the methanol pool flames with diameters substantially less than 3 cm. Even for the larger diameter pools, there is always a region near the pool edge where $r_o - r$ is sufficiently small so that such a steady flame is continuously maintained. This edge flame constitutes the holding edge.

Now for the large-diameter flames, values of $r_o - r$ will be large in the central regions of the fuel stream, and there will be very little mixing in the central stream until the fuel rises to a very large distance above the pool surface. If it were possible for the burning velocity to adjust continuously so that very low values of S_f were permissible in these central regions, then the product $S_f(r_o - r)$ could still be low and τ-value could always be small enough to insure a steady-state flame structure. (Such flames would be of enormous height.) However, as indicated, the very existence of flammability limits at finite fuel concentrations is caused by the competition between combustion and buoyancy forces, and this competition results in the presence of a discontinuity in burning velocity at the limit. Thus combustion waves will not propagate at all (in the horizontal direction) if flame speeds are less than about 30 cm sec^{-1}. Thus, the S_f value is not continuously adjustable and there is a minimum below which a steady-stage flame cannot exist. With this minimum value for S_f for the large-diameter pools,

the τ-ratio will necessarily be large in the central regions of the fuel stream. This means that in these central regions of the large pool flames, the flammable volume is generated at too slow a rate by molecular diffusion to keep up with its minimal rate of consumption at the limits of flammability.

However, the flow disturbances created in the wake of the combustion wave by the combustion force flow expansion and by the buoyancy force couple can promote convective mixing: a new and more effective mixing process. There may, however, be a delay between the passage of the wave and the regeneration of a new flammable volume by convective mixing. It is this cross-coupling between the two processes that now controls the overall burning rate process and that causes large-amplitude radiance oscillations at pool diameters in excess of 9 cm. In the transition zone between 3 and 9 cm, the amplitude of the oscillation is clearly dependent on the τ-ratio. If we consider a pool of a given size in which the radial distance is a variable, then each fuel element flowing from the pool surface has its individual value for the τ-ratio. Near the edge of the fuel stream the ratio is small, and hence a continuous flame is present at this holding edge. Near the axis of a pool of large enough diameter, the τ-ratio will be sufficiently large so that a premixed flammable volume does not exist in steady state because the diffusive mixing process is too slow relative to the convective mixing rate. A self-sustained oscillation could then appear in the central regions of such a flame via the mechanism described above. In small pools, where the τ-ratio is small for most of the cross-sectional area of fuel stream, the oscillations are small in amplitude and confined to the central stream tubes only. For the larger pools where the τ-ratio is large for most of the cross section, the oscillations are large in amplitude and cover almost the entire pool area. For these larger pools, the combustion-induced convective mixing process would be controlling.

Finally, for still larger diameter pools (or in the presence of fluctuating, forced-convective flows) the combustion waves traversing different portions of the pool propagate independently. There would then be a random distribution of phases, and the flame would appear turbulent.

Starting with the simple postulate that the observed oscillations are caused by ignition, propagation, mixing, and reignition cycles within the finite flammable volume above the fuel surface, it is possible to predict oscillation frequencies and compare these with the data presented. The oscillation frequency should then be simply related to the reciprocal of the time required for a combustion wave, ignited at the edge, to propagate inward to the axis of the pool. This propagation wave would constitute the initial part of the cycle of oscillation which consumes the flammable volume and generates a maximum in the burned gas volume and/or temperature of the flame or fireball. Once consumed and converted to combustion products, this fireball shields the remaining fuel volume (whose composition is above the rich limit) from the surrounding air volume (whose composition is below the lean limit). This burned gas fireball must rise, convected upward as part of the buoyant plume, before a new flammable volume can be regenerated and reignited. The radiance-growth phase of the oscillation is thus associated with the propagation portion of the cycle, whereas the radiance-decay phase is associated with the upward convection, entrainment-cooling-remixing portion of the cycle. The two

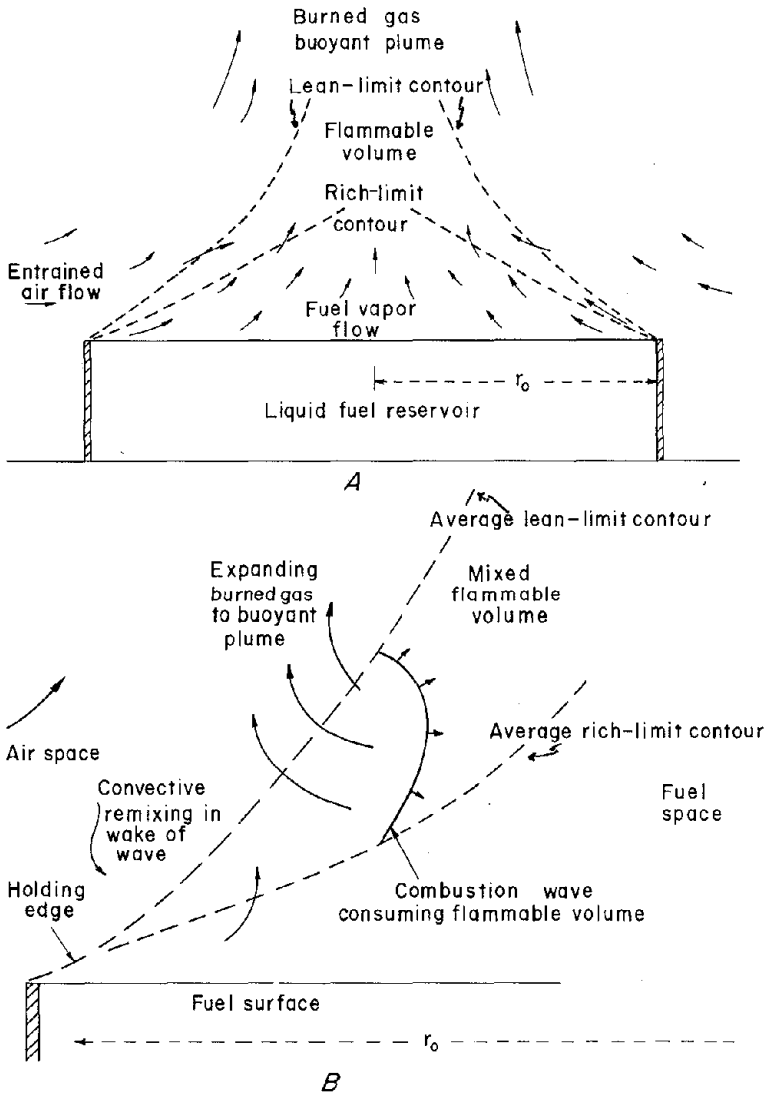

FIGURE 8. - Flame oscillations depicted as contiguous combustion waves consuming the flammable volume in propagation and convective-remixing cycles.

cycles need not be clearly separated to the observer at a large distance from the flame. The convection-cooling phase near the edges of the pool could overlap in time with the propagation phase in the central regions.

Now clearly, the detailed fluid dynamical interaction between the propagation phase and the buoyancy-induced remixing phase is a complex problem whose solution awaits a far more accurate description of the real flow field of a pool flame than has heretofore been available in the literature. Figure 8 shows the geometry involved. In figure 8A an attempt is made to sketch the flow velocity structure and the lean- and rich-limit contours that define the flammable volume. In figure 8B the holding edge is delineated and an attempt is made to sketch the propagating wave during part of its propagation cycle. Clearly, the geometric factors that control the flame speed S_f and the overall velocity field $v_b(r, z, t)$ under the combined influence of the combustion force expansion and the buoyancy force couple are very complicated. In the estimates to be presented, these factors will be necessarily oversimplified. In addition, the assumption will be made that the propagation portion of the cycle and the convective-entrainment-remixing portion of the cycle overlap precisely in time. This is an oversimplification; in reality, the cycles can lag substantially since the convective mixing and the buoyant rise rates may, in some instances, be slower than the propagation rate.

Despite these limitations, it is possible to make some quantitative estimates. Assume that the holding edge is continuously attached to the flammable volume at the point where fuel flow and the entrained air flow first meet.

The wave is assumed to propagate inward and upward from this holding edge. The actual propagation direction is determined by the average angle that the flammability limit contours make with the horizontal. We assume that for the larger pools, the angle is nearly horizontal. For the smaller pools this is not accurate, but the larger distance of travel is partly compensated for by the finite thickness of the holding edge. The speed of horizontal propagation for free space propagation of a combustion wave through near-limit mixtures is simply $S_f = (S_u)_a \rho_u/\rho_b$. The quantity $(S_u)_a$ is the limit burning velocity for quenching by natural convection (9), and its value is typically about 6 cm sec^{-1}. For near-limit mixtures $\rho_u/\rho_b \simeq 5$ and hence S_f (limit) $\simeq$ 30 cm sec^{-1}. Thus the time associated with the propagation half cycle is simply

$$\tau_{propagation} \simeq r_o/S_f . \tag{16}$$

If the remixing process occurs in the immediate wake or in advance of the propagation wave, then it may be assumed that the two half cycles nearly overlap. In this case, the oscillation frequency is simply

$$f_p = \frac{1}{\tau_{propagation}} = \frac{S_f}{r_o} = \frac{30}{r_o} . \tag{17}$$

In this instance, the peak in the radiance signal would be associated with the time of arrival of the wave in the regions where the available flammable volume is the largest. These estimates of the oscillation frequencies are plotted in figure 9 and are about the correct order of magnitude. Clearly, however, the curve overestimates the frequencies for pool diameters between 4 and 20 cm. It also grossly underestimates frequencies for diameters in excess of 20 cm. The overestimate for the small pools is probably caused by the neglect of the upward component of the distance the wave must travel to reach the center of the flammable volume.

To correct for the underestimate for the large-diameter pools, a refinement should be made by considering the induced convective velocities. We simplify somewhat the problem of determining these convectively induced velocities as follows:

As derived earlier, the buoyant rise velocity for the center of mass of a spherically propagating fireball in a premixed gas is given by

$$v_b = \frac{1}{4}\left(\frac{\rho_u - \rho_b}{\rho_u + \rho_b}\right)\frac{gr}{S_b} .$$

The net motion of the spherical fireball is upward, whereas the net motion of an equivalent volume of cold surroundings is downward at the same velocity. Near the top of the fireball, however, the surroundings move outward (parting, as it would to make way for a rising balloon). In the equatorial regions the cold gas motion is downward as required by the buoyancy force couple. Near the bottom of the fireball, the surroundings move inward to occupy the space being vacated by the rising fireball.

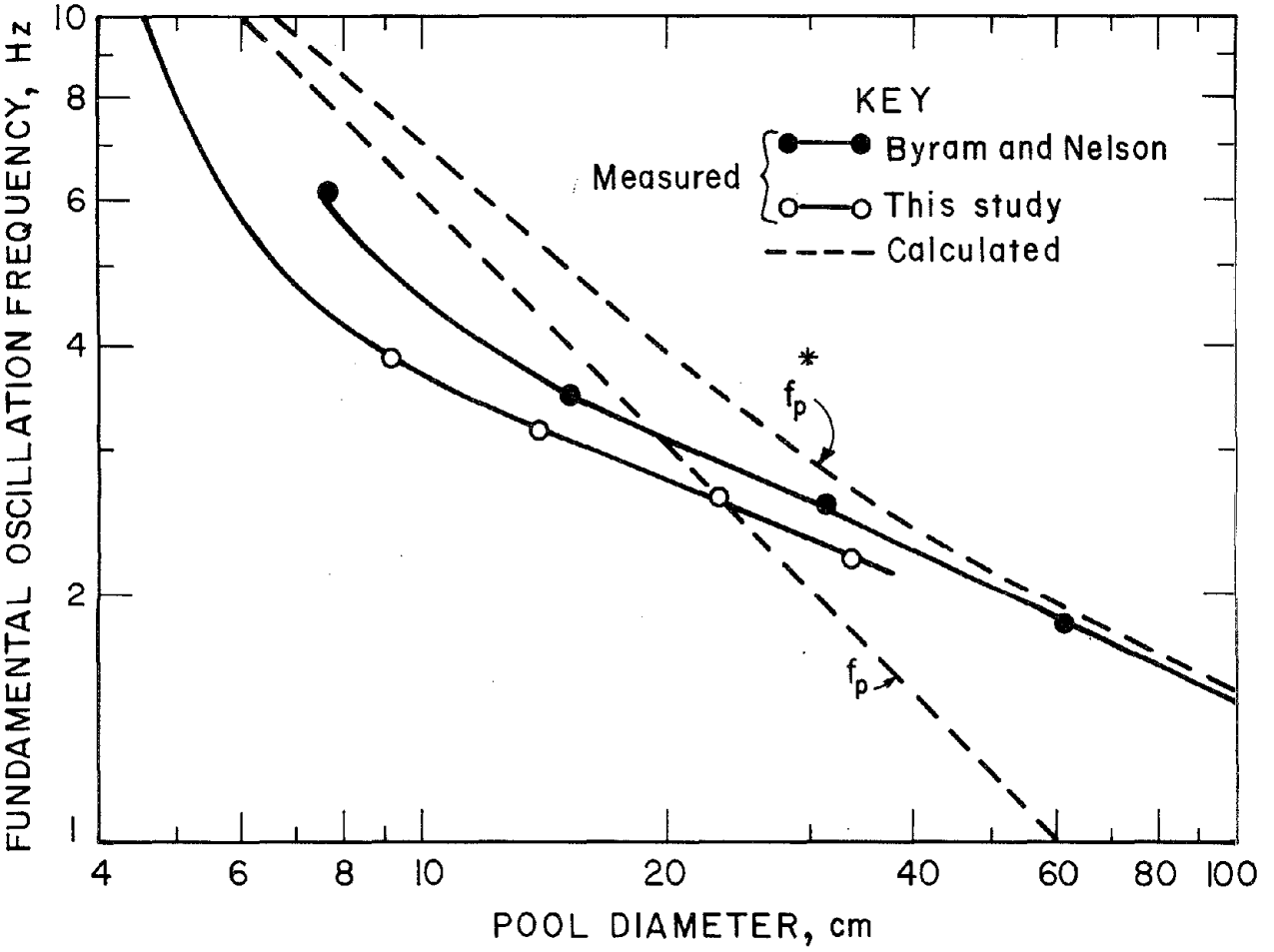

FIGURE 9. - Calculated oscillation frequencies for combustion wave cycles, with (f_p^*) and without (f_p) inward convective flow, compared with the data.

If we associate the fireball with the burned gas flame volume above the pool, then r is proportional to r_o, the pool radius. The propagation process in the diffusion flame is always near the bottom of this "fireball." Hence the convective velocity of unburned gas is always inward, and this is in the direction of propagation from the holding edge. We assume that this average inward component is some fraction of v_b. Actually it may be a relatively large fraction of v_b near the holding edge, but since all inward flows meet at the pool axis, the inward component is necessarily zero at the pool axis where these flows converge. This gives

$$\bar{v} \text{ (inward)} = \beta\, v_b, \tag{18}$$

where β is a proportionality constant, substantially less than unity, that includes both the flow-component averaging process and the geometric factor relating pool radius r_o to fireball radius r. The inward flame speed of propagation from the holding edge is therefore

$$S_f = S_b \text{ (limit)} + \bar{v} \text{ (inward)}. \tag{19}$$

The combustion wave thus rides on top of some average inward convective velocity as it propagates from the holding edge to the center of the flammable volume. Hence the oscillation frequency is

$$f_p^* = \frac{S_f}{r_o} = \frac{S_b \text{ (limit)}}{r_o} + \frac{\beta}{4}\left(\frac{\rho_u - \rho_b}{\rho_u + \rho_b}\right)\frac{g}{S_b \text{ (limit)}}. \qquad (20)$$

We compare the predicted value of f * with the measured value in figure 9. The β value has been taken as $\beta = 0.17$ and S_b as 30 cm sec^{-1}. The agreement is somewhat better now for the larger pool diameters than that obtained by the f_p value, which neglected inward convective velocities. A more accurate refinement awaits a more accurate description of the real convective flow field for such flames.

In any case, it is important to emphasize the close coupling of the two processes of propagation and convection for such flames. As indicated earlier, not only does convection promote the mixing of fuel and air streams, but the very existence of flammability limits, and the corresponding composition contours that define a flammable volume, is itself a reflection of the competitive interaction of combustion and buoyancy forces.

Thus, buoyancy or natural convection plays a dual role. It is both a catalyst and a quenching agent. It is essential for propagation in the larger diameter pools because it promotes the mixing of fuel and air streams; however, in the mixed or mixing regions, it limits the size of the flammable volume, extinguishing by flame stretch all waves that tend to propagate beyond the limit contours at burning velocities less than some critical value.

LARGE-SCALE LIMITING RATES FOR POOL FLAMES

The rate of combustion of a liquid pool flame is determined by the rate of heat feedback to the fuel reservoir from the exothermic reaction zone and the burned gas fireball it generates. For large-diameter pools, the significant mode of heat transfer is radiation in the infrared (11-12). For the largest diameter flames, the rate attains a maximum value, independent of size, when the flame becomes optically thick and shape factors attain their limiting values (10). For such a pool under radiative control the limiting value of the liquid surface regression rate is

$$v_\ell = \frac{\frac{1}{2}\, e_f\ (h)\ F_{f\to\ell}\ \sigma\ \bar{T}_f^{\,4}}{\rho_\ell\ (C_a T_s - C_\ell T_u + \Delta H_v)}. \qquad (21)$$

This formula is obtained by transforming the fireball volume into an idealized effective "flame surface" of constant emissivity. The quantity e_f (h) is the flame emissivity as viewed by the perfectly absorbing fuel reservoir, and $F_{f\to\ell}$ is a shape factor. The burned gases are characterized by some average temperature $\bar{T}_f$. The density of liquid fuel is ρ_ℓ, and ΔH_v is its heat of vaporization. The heat capacities of the vaporizing fuel and the liquid fuel reservoir are C_a and C_ℓ, respectively, and T_s and T_u are their respective temperatures.

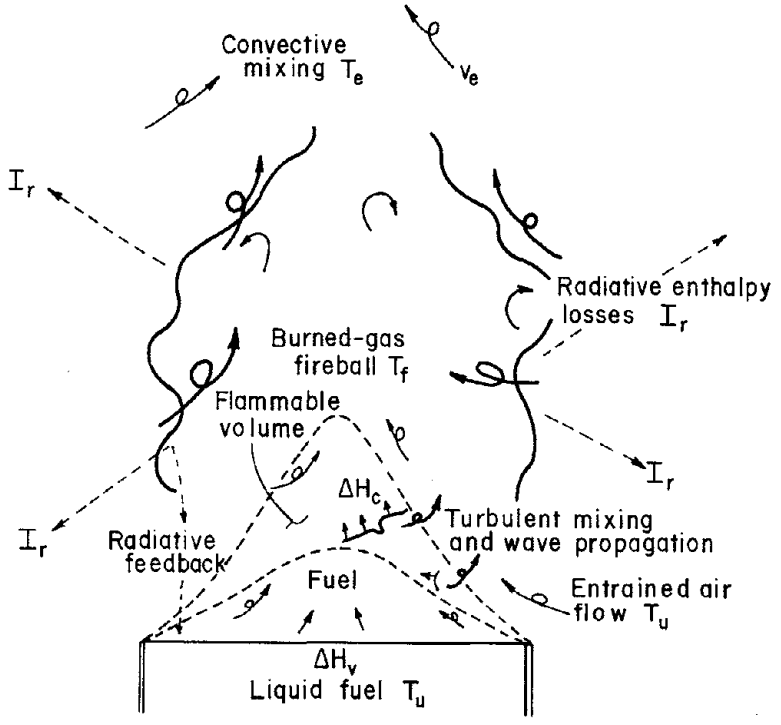

FIGURE 10. - Structure of a turbulent diffusion flame above a large pool.

Now Burgess, Grumer, and Wolfhard (4) first noted the existence of an empirical correlation between the maximum burning rate for a horizontal pool of very large size and the ratio of its heat of combustion to heat of vaporization. It is instructive to derive this Burgess-Grumer-Wolfhard law from considerations of the overall enthalpy balance in the system, in order to be aware of the parameters that determine the magnitude of this limiting rate.

The structure of the turbulent diffusion flame above a large pool is delineated in figure 10. The flow is turbulent, and the combustion waves traversing through the flammable volume in the fireball boundary layer are randomly distributed in time and space. This turbulent, random distribution of phases causes the mixing of fuel and air to occur within turbulent eddies whose scale is much smaller than the pool dimensions. The time-average position of the flammable volume is depicted, as is the fireball volume.

Now consider the overall enthalpy balance for the system. The unburned liquid fuel is initially at T_u, and it absorbs energy from the flame to sustain its vaporization rate. These vapors mix with entrained air to generate a flammable volume. Combustion waves propagate through this volume, generating sensible heat in the combustion products from the potential energy of the combustion reaction. These burned gas products eventually lose all of this energy to the surroundings by radiation and convective mixing. However, a small portion of this energy feeds back to reactants to sustain evaporation, mixing, and combustion before it is finally lost to the surroundings. The source of enthalpy is the combustion process. Its rate of generation in the flammable volume is assumed, as before, to be governed by the horizontal limit burning velocity. This is the minimum velocity at which unburned gas can be consumed, since all lower velocities would be discontinuously quenched by buoyant convection (9). This minimum velocity is

$$(S_u)_a = [2 \alpha g \rho_b/\rho_u]^{1/3}, \qquad (22)$$

where α is the spatially averaged or effective diffusivity in the flame front. If the average mass concentration of fuel in the flammable volume is M, and

the heat of combustion per unit mass of fuel is ΔH_c, then the rate of generation of combustion enthalpy per unit area of unburned gas being traversed by the wave is $(S_u)_a$ M ΔH_c. The combustion products, containing this combustion enthalpy in the form of sensible heat, expand and convect upward into the buoyant plume, generating the burned gas fireball. Initially these burned gases are near the adiabatic flame temperature for the near-limit mixtures that comprise the flammable volume. Since this temperature (~1,500° K) is much hotter than the surroundings, and the fireball is large enough to be optically thick, some of this enthalpy is radiated to the surroundings. A portion of the surroundings consists of the unburned gases, their pyrolysis products (soot), the fuel reservoir, and its container. These absorb some fraction of this radiating enthalpy. These burned gases may be characterized by an average temperature $\bar{T}_f$ and an average emissivity ϵ_f. The radiating enthalpy per unit area of flame surface is $I_r = \bar{\epsilon}_f \sigma \bar{T}_f^4$, where $\bar{\epsilon}_f$ is the average emissivity of the effective flame surface, as viewed from the surroundings.

The fireball volume, which is at the base of the buoyant plume, is continuously cooled as it radiates to the surroundings and mixes with entrained air. At some point in this cooling process, the convective entrainment losses become more significant than radiation. Conceptually, it is easiest to assume that this transition occurs abruptly at some characteristic plume temperature $\bar{T}_e$. Practically, it is at some height in the plume where the average temperature is so low that convective heat transfer with the surroundings exceeds the radiative loss component. This height may be close to the visually measured flame height for the sooty flames. However, for the clean alcohol or hydrogen flames, it is probably well above the measured height.

In any case, the transition should be rather abrupt because of the strong temperature dependence of the radiative component. If the average plume density is ρ_e, the average heat capacity is $\bar{c}$, and the average mixing velocity into the surroundings is $\bar{v}_c$, then the convective loss per unit area is $I_c = \bar{c}\, \rho_e \bar{v}_c\, (\bar{T}_e - T_u)$. Conserving the enthalpy by balancing the generation rate with the loss rate gives

$$(S_u)_a \; M \; \Delta H_c = I_r + I_c . \tag{23}$$

The fraction of combustion energy radiating to the surroundings is then

$$f = \frac{I_r}{I_r + I_c} = \frac{\bar{\epsilon}_f \sigma \bar{T}_f^4}{\bar{\epsilon}_f \sigma \bar{T}_f^4 + c\, \rho_e\, \bar{v}_c\, (T_e - T_u)} . \tag{24}$$

Eliminating $\sigma \bar{T}_f^4$ and I_c from equations 21-24 and noting that $\Delta H_v \gg C_a T_s - C_\ell T_u$ for most pool flames, one obtains

$$v_\ell \rho_\ell = \dot{m}'' = \beta \; \Delta H_c / \Delta H_v \tag{25}$$

where

$$\beta = \frac{1}{2} f \frac{\bar{\epsilon}_f(h)}{\bar{\epsilon}_f} M F_{f \to \ell} \left[2 \alpha g \rho_b / \rho_u \right]^{1/3} . \tag{26}$$

Equation 25 is then the Burgess-Grumer-Wolfhard law, which relates the limiting value of the mass burning rate for a large pool to the ratio $\Delta H_c/\Delta H_v$. Note that the proportionality constant β varies linearly with the following: the fraction of combustion power radiating to the surroundings, an emissivity anisotropy factor, the average fuel concentration in the flammable volume, the flame-to-pool shape factor, and the limit burning velocity.

For typical hydrocarbon flames, $\rho_\ell = 0.75$ g cm^{-3}, $F_{f\to\ell} \simeq 0.40$, $f = 0.50$, $M = 0.96 \times 10^{-4}$ g cm^{-3}, $e_f(h)/\overline{e_f} \simeq 1.5$, and $(S_u)_a \simeq 6.0$ cm sec^{-1}. Hence one obtains $\beta = 0.51 \times 10^{-2}$ g cm^{-2} min^{-1}. This is in fair agreement with measured values (5, 11).

RADIANCE DATA FROM A SMALL METHANOL POOL FLAME

It is instructive to describe some experimental measurements obtained on the radiative balance from a methanol pool flame. A 14-cm-diameter-pool flame of methanol was used to study the angular dependence of the emitted radiation. The radiance was measured with a BiAg thermopile with a CaF_2 window. The thermopile was located 1.5 meters from the center of the pool surface. The angular dependence of the radiance was measured by rotating the thermopile about an arc in a vertical plane so as to view the emitted radiation at various angles above and below the liquid fuel surface. The geometry of the system is depicted in figure 11. The thermopile was pivoted about the pool center at an angle θ with respect to the horizontal, and the radiance was measured as a function of this viewing angle. The measured irradiance at the detector for each viewing angle is shown in column 2 of table 1. As indicated in figure 11, the measurements were made at a fixed distance $r = 150$ cm from the center of the pool surface. However, the center of emission of the fireball was determined to be at a height of $\delta = 25$ cm above this reference point. Thus, as can be seen from the figure, the distance of the thermopile from the center of emission was actually

$$d = [r^2 + \delta^2 - 2\delta r \sin\theta]^{1/2}. \tag{27}$$

The appropriate d^2/r^2 correction factor for the radiance is shown in the third column of the table, and the corrected irradiance signal at the detector is shown in the fourth column. There is also a correction factor $\Delta\theta$ to the measured angle, and as can be seen from the figure, the corrected angle (shown in column 5) is

$$\theta_c = \theta - \arctan\frac{\delta\cos\theta}{r - \delta\sin\theta}. \tag{28}$$

The corrected irradiance is finally shown as a function of the corrected angle in figure 12. Clearly, when properly referenced to the center of emission of the fireball, the radiance from the flame is spherically symmetrical at all viewing angles above the pool surface. As one descends below the pool surface, an increasing fraction of the fireball's radiance is intercepted by the liquid pool reservoir and its container. When viewed from below at $\theta = -90°$, the fireball radiance is almost completely blocked by the pool and its container. If one assumes that the radiance would be spherically symmetrical in the

absence of the pool reservoir and its container and that all of the radiance intercepted by reservoir and container is absorbed, then it is possible to calculate the fraction of radiant energy that feeds back to the pool and its container. This fraction of radiant energy that is fed back to the fuel to sustain the combustion process is 10% for the pool studied. Hence, some 90% of the radiant energy emitted by the fireball escapes to the surroundings. The volume of methanol used for each experiment was 100 cm^3, and the average burning time was 9.46±0.35 min, giving a volumetric consumption rate of 0.176 $cm^3\ sec^{-1}$. For the pool's surface area of 154 cm^2, the average surface regression rate was $v_\ell = 0.0686$ cm min^{-1}. The fraction of combustion energy radiating to the surroundings is therefore

$$f = 0.90\,\frac{4\pi r^2 H}{\dot{V}\rho_\ell \Delta H_c}\,, \tag{29}$$

where $\dot{V}$ is the volumetric consumption rate of the liquid fuel and H is the symmetric value of the measured radiance (in the upper hemisphere) measured at the distance r. For the above value of $\dot{V}$, ρ_ℓ = 0.79 g cm^{-3}, ΔH_c = 170.9 kcal $mole^{-1}$ (2.235×10^4 j gm^{-1}), H = 1,725 μw cm^{-2}, and r = 150 cm, one obtains f = 0.14. That is, the fraction of combustion energy that is lost by radiation to the surroundings is 14%.

TABLE 1. - Measured, vertical angular distribution of the radiance from a methanol pool flame

Viewing angle (θ), degrees above the horizontal	Measured irradiance, μw cm^{-2}	Correction factor $1-\frac{2\delta}{r}\sin\theta+\left(\frac{\delta}{r}\right)^2$	Corrected irradiance, μw cm^{-2}	Corrected viewing angle $(\theta)_c$, degrees
-87.5	276	1.367	377	-88
-45	760	1.268	960	-53
-24	1,270	1.166	1,480	-32
0	1,680	1.029	1,730	-10
45	2,160	.789	1,700	37
65	2,390	.722	1,730	60
90	2,530	.690	1,750	90

The 14-cm-diameter pool is relatively small, and both the combustion rate and the radiance are far from their limiting values for large diameters. For larger pools, as they approach their limiting values, an equipartition condition is attained between convective and radiative losses, and $f \to 0.5$.

It is possible to calculate the flame to pool shape factor $F_{f\to\ell}$ from the data obtained. The radiance from the flame fireball is $\epsilon_f \sigma \bar{T}_f^4$. The radiance intercepted by the fuel reservoir (and its container) is $1/2\ \epsilon_f(h)\ F_{f\to\ell}\ \sigma\bar{T}_f^4$. The fraction of radiant energy emitted by the fireball that is intercepted by the fuel reservoir is therefore

$$\phi = \frac{1}{2}\,\frac{\epsilon_f(h)}{\bar{\epsilon}_f}\,F_{f\to\ell}. \tag{3}$$

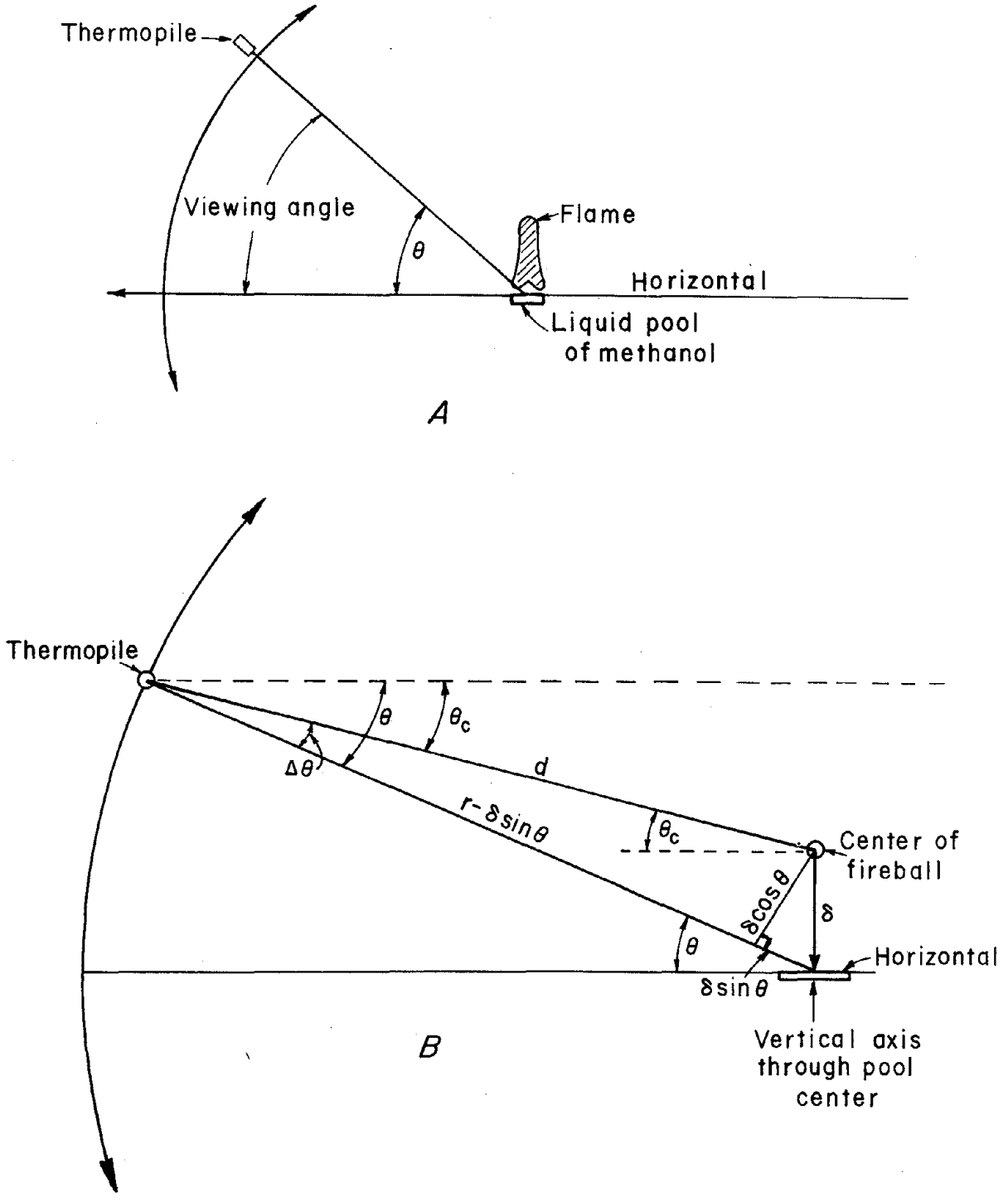

FIGURE 11. - *A*, Geometry used to measure the angular dependence of the pool flame radiance; *B*, correctional geometry needed to reference radiance and viewing angle to the center of the fireball from the center of the pool.

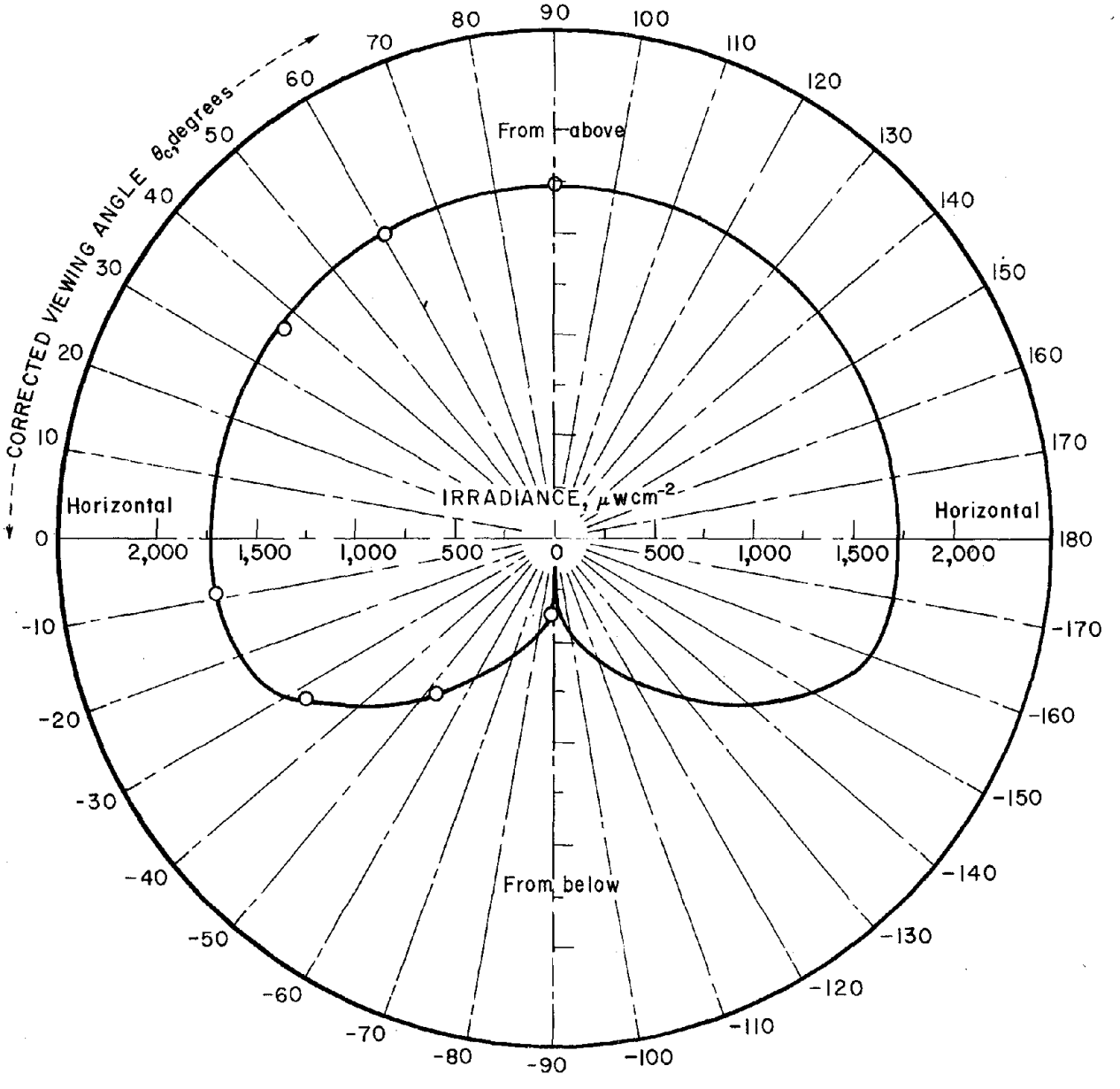

FIGURE 12. - Measured irradiance as a function of viewing angle referenced to the center of the fireball for a 14-cm-diameter methanol pool flame.

But this fraction was measured to be $\Phi = 0.10$, and hence

$$F_{f \to \ell} = 0.20 \frac{\bar{\epsilon}_f}{\epsilon_f (h)} . \tag{31}$$

Now the far-field flame emissivity, as viewed by the surroundings, is $\bar{\epsilon}_f$, and this is associated with the plume or pool diameter. The near-field emissivity, as viewed by the pool, is associated with the flame or plume height. For this

small, relatively thin flame, $\epsilon = 1 - e^{-k\bar{x}} \simeq kx$ where $\bar{x}$ is the characteristic dimension. Thus

$$\frac{\epsilon_f}{\epsilon_f(h)} \simeq \frac{d}{h} \tag{32}$$

so that the emissivity anisotropy factor is approximated by the height-to-diameter ratio. For the methanol pool used, the center of radiant emission was measured to be at $\delta = 25$ cm. Subtracting the small average distance of the unburned fuel space and doubling gives an average flame height of approximately 40 cm, and hence one obtains $d/h \simeq 14/40 = 0.35$. This gives $F_{f\to\ell} \simeq 0.072$. This is reasonably consistent with the shape factor one would calculate for an effective flame surface at a height of $\delta = 25$ cm from a pool of 14-cm diameter.

This shape factor is also relatively small, compared to the maximum values of $F_{f\to\ell} \simeq 0.40$ that would pertain to the very large diameter pools. But it is this small shape factor that mainly accounts for the small fraction of radiant energy that is fed back to the fuel surface. For these small-diameter pools, the emissive fireball sits high above the pool, and the fuel intercepts only a small fraction of the emitted radiance.

Since the magnitude of the radiance was measured at a known distance r, it is possible to estimate the flame emissivity from the equation

$$H = \frac{\bar{r}_f^{\,2}}{r^2}\,\bar{\epsilon}_f\,\sigma\,T_f^{\,4}. \tag{33}$$

For an equivalent flame radius $\bar{r}_f$, somewhat larger than the pool radius, and setting $\bar{T}_f \simeq 1{,}300°$ K, one obtains $\epsilon_f \simeq 0.03$. It is this small far-field emissivity that accounts for the fact that only 14% of the combustion energy is radiated to the surroundings rather than the 50% that is radiated for very large diameter pools. Note, however, that with $h/d = 2.86$, the near-field emissivity, as viewed by the pool, is significantly larger; namely, $\epsilon_f(h) \simeq 0.09$.

SUMMARY

After a brief critique of past theories of diffusion-flame structure, the problem that is central to this report was considered; namely, the role played by buoyancy or buoyant convection in controlling the structure and dynamics of diffusion flames. A variety of experimental and theoretical studies were then described, and the attempt to synthesize these studies into a coherent pattern led to the formulation of an entirely new view of the structure and dynamics of such flames.

A beginning was made toward the realistic treatment of natural convection in combustion processes by considering the effect of the buoyancy force couple on the motions of burned and unburned gases in a premixed system. An equation was derived for the maximum free convective velocity of a spherically

expanding fireball, which gave predictions that compared favorably with the available data. This led to the concept of a buoyancy-induced Reynolds number that was used to estimate the behavior of the mixing flows in the flammable volume just above the surface of a burning liquid pool.

The experimental studies reported were the infrared radiance oscillations of methanol pool flames of varying sizes, including their fundamental flicker frequencies and their oscillation amplitudes. The measured frequencies compared favorably with theoretical predictions, which assume that combustion waves propagate contiguously from a holding edge at the rim of the pool to the center of the flammable volume above the axis of the pool. This new view is at variance with the traditional ones which assume either uniform reaction throughout the diffusive mixing zone, or infinitely rapid reaction at the stoichiometric contour surface. Instead, combustion waves are viewed as propagating contiguously through a flammable volume defined by the lean- and rich-limit contour surfaces, while complementary portions of that volume are being regenerated by convective mixing. The measured, coherent, radiance oscillations are thus the direct manifestations of these propagation and mixing cycles. Although the good agreement between predicted and measured flicker frequencies tends to confirm this new viewpoint, there are additional factors that were not included in this simplified theory. A more accurate theory awaits a more complete description of the real, time-dependent flow field for such flames. Nevertheless, in view of these considerations, future refinements must recognize the significance of the role played by buoyant convection and its <u>duality</u>, in both aiding and impeding flame propagation.

Next, consideration was given to the overall energy balance for very large pool flames. Using this new viewpoint of buoyancy's dual role, it was possible to derive a realistic equation for the limiting burning rate for such large flames that is in reasonable agreement with the empirical law of Burgess, Grumer, and Wolfhard. Finally, data were presented on the angular dependence of the absolute radiant emittance of a small pool flame. The analysis of the data provided some insights into the factors that controlled its overall energy balance.

REFERENCES[5]

1. Altenkirch, R. A., Eickhorn, N. N. Hsu, A. B. Brancic, and N. E. Cevallos. Characteristics of Laminar Gas Jet Diffusion Flames Under the Influence of Elevated Gravity. 16th Combustion Symp., MIT, Cambridge, Mass., Aug. 15-21, 1976. The Combustion Institute, Pittsburgh, Pa., 1977, pp. 1165-1174.

2. Barr, J. Diffusion Flames. 4th Combustion Symp., MIT, Cambridge, Mass., Sept. 1-5, 1952. The Williams and Wilkins Co., Baltimore, Md., 1953, pp. 765-771.

3. Blinov, V. I., and G. N. Khudiakov. (Diffusive Burning of Liquids.) Izdatel'stvo Akad. Nauk SSSR, Moscow, 1961, pp. 64-69; translation 2093 pub. by Office of Technical Services, U.S. Dept. of Commerce.

4. Burgess, D., J. Grumer, and H. G. Wolfhard. Burning Rates of Liquid Fuels in Large and Small Open Trays. Article in The Use of Models in Fire Research. Nat. Acad. Sci.-Nat. Res. Council, Pub. 786, 1961, pp. 68-75.

5. Burgess, D., and M. Hertzberg. Radiation From Pool Flames. Ch. 27 in Heat Transfer in Flames, ed. by N. Afgan and J. Beer. Scripts Book Co., Washington, D.C., 1974, pp. 413-430.

6. Burke, S. P., and T. E. N. Schumann. Diffusion Flames. Proc. 1st Combustion Symp. (76th ACS Meeting), Swampscott, Mass., Sept. 10-14, 1928. The Combustion Institute, Pittsburgh, Pa., 1965, pp. 2-11.

7. Byram, G. M., and R. M. Nelson, Jr. The Modeling of Pulsating Fires. Fire Technol., v. 6, No. 2, May 1970, pp. 102-110.

8. Chamberlin, D. S., and A. Rose. The Flicker of Luminous Flames. Proc. 1st Combustion Symp. (76th ACS Meeting), Swampscott, Mass., Sept. 10-14, 1928. The Combustion Institute, Pittsburgh, Pa., 1965, pp. 27-32.

9. Hertzberg, M. The Theory of Flammability Limits. Natural Convection. BuMines RI 8127, 1976, 15 pp.

10. _____. The Theory of Free Ambient Flames. The Convectively Mixed Combustion of Fuel Reservoirs. Combustion and Flame, v. 21, 1973, pp. 195-209.

11. Hertzberg, M., C. D. Litton, W. F. Donaldson, and D. Burgess. The Infrared Radiance and the Optical Detection of Fires and Explosions. 15th Combustion Symp., Tokyo, Japan, Aug. 25-31, 1974. The Combustion Institute, Pittsburgh, Pa., 1974, pp. 137-144.

[5]Titles enclosed in parentheses are translations from the language in which the item was published.

12. Hottel, H. C. Review of 'Certain Laws Governing Diffusive Burning of Liquids," by V. I. Blinov and G. H. Khudiakov. Fire Res. Abs. and Reviews, v. 1, No. 2, January 1959, p. 41.

13. Hottel, H. C., and N. R. Hawthorne. Diffusion in Laminar Flame Jets. 3d Combustion Symp., Madison, Wis., Sept. 7-11, 1948. The Williams and Wilkins Co., Baltimore, Md., 1949, pp. 266-288.

14. Maklakov, A. I. (Fluctuations of Diffusion Flames Arising in the Laminar Regime of Fuel Flow.) Zhur. Fiz. Khim., v. 30, 1956, p. 708.

15. Margolin, A. D., V. P. Karpov, and E. S. Severin. (Laws Governing the Rise of a Sphere of Products With the Combustion of Near Limit Mixtures.) Fiz. Goreniya Vzryva, v. 9, No. 6, 1973, pp. 755-758.

16. Sapko, M. J., A. L. Furno, and J. M. Kuchta. Flame and Pressure Development of Large-Scale CH_4-Air-N_2 Explosions. Buoyancy Effects and Venting Requirements. BuMines RI 8176, 1976, 32 pp.

17. Savage, D. L. The Enclosed Laminar Diffusion Flame. Combustion and Flame, v. 6, 1962, pp. 77-87.

18. Schlichting, H. Boundary Layer Theory. McGraw-Hill Book Co., Inc., New York, 6th ed., 1968, pp. 38, 162, 540.

19. Sibulkin, M., and A. G. Hansen. Experimental Study of Flame Spreading Over a Horizontal Fuel Surface. Combustion Sci. and Technol., v. 10, 1975, pp. 85-92.

20. Wohl, K., C. Gazley, and N. Kapp. Diffusion Flame. 3d Combustion Symp., Madison, Wis., Sept. 7-11, 1948. The Williams and Wilkins Co., Baltimore, Md., 1949, pp. 288-300.

*U.S. GOVERNMENT PRINTING OFFICE: 1978-703-103/19 INT.-BU.OF MINES,PGH.,PA. 22731

BIBLIOGRAPHIC DATA SHEET	1. Report No. BuMines RI 8263	2.	PB277250

4. Title and Subtitle: The Diffusion Flame in Free Convection. Buoyancy-Induced Flows, Oscillations, Radiative Balance, and Large-Scale Limiting Rates	5. Report Date
	6. Performing Organization Code
7. Author(s): M. Hertzberg, K. Cashdollar, C. Litton and D. Burgess	8. Performing Organization Rept. No.
9. Performing Organization Name and Address: Pittsburgh Mining and Safety Research Center, Bureau of Mines, USDI, 4800 Forbes Avenue, Pittsburgh, PA 15213	10. Project/Task/Work Unit No.
	11. Contract/Grant No.
12. Sponsoring Agency Name and Address: Office of Assistant Director--Mining, Bureau of Mines, USDI, 2401 E Street, NW, Washington, DC 20241	13. Type of Report & Period Covered: RI, Research FY 77
	14. Sponsoring Agency Code

15. Supplementary Notes

16. Abstracts: A variety of experimental and theoretical studies of diffusion flames in free convection are described in this Bureau of Mines report. The cross-coupling between buoyancy-induced flows and the combustion process is explored as it relates to the size, structure and radiative balance of flames. A critique of classical diffusion flame studies is first presented. The buoyancy force-couple is then introduced and an equation is derived for the maximum free convective velocity of an expanding combustion wave. New data are presented for the size-dependent radiance oscillations of diffusion flames. Data are also presented for the angular distribution of the total radiant intensity from a small methanol pool flame. Both the amplitude and frequency of the measured oscillations are compared with theoretical predictions that are based on a new view of the structure of diffusion flames. This new view is at variance with the traditional one which assumes uniform reaction in the diffusive mixing zone.

17. Key Words and Document Analysis. 17a. Descriptors

Flames, diffusion flames, convection, buoyancy, flame propagation, combustion, burning rate, turbulent mixing, radiant emittance, oscillations.

17b. Identifiers/Open-Ended Terms

Free convection in diffusion flames; Buoyant rise velocities; Buoyancy-induced Reynolds number; Flame flicker frequencies; Radiance oscillations; Large pool flames under radiative control.

17c. COSATI Field/Group: Propulsion and fuels; Combustion; Physics, Fluid mechanics; Aerodynamics. 20D; 21B

18. Distribution Statement	19. Security Class (This Report)	21. No. of Pages
Release unlimited by NTIS.	UNCLASSIFIED	39
	20. Security Class (This Page) UNCLASSIFIED	22. Price PCA03/MA01